EDITORIAL BOARD

Please consider, when preparing the manuscript, the *Instructions for the Authors* at the end of each issue. Orders, exchange for other journals, manuscripts and all correspondences concerning off prints should be sent to the Executive Editors or to the editorial secretaries at the address:

Contents

ON THE NORMAL FORM OF DOUBLE–HOPF BIFURCATION

Gheorghe ŢIGAN, Emanuel CISMAŞ,
Stelian MIHALAŞ, Oana BRANDIBUR

Abstract

A study on degenerate normal form of double-Hopf bifurcation is performed. This bifurcation is met in differential systems of dimension at least four and with minimum two independent parameters. We obtain bifurcation diagrams for amplitude system when one or two generic conditions are eliminated. [1]

Keywords and phrases: *dynamical systems, bifurcations, normal forms*

1 Introduction

In this work we aim to present a study related to normal form of double-Hopf bifurcation in generic four-dimensional differential system. A double-Hopf bifurcation arises in the following way. Let

$$\dot{x} = f(x, \alpha), \quad x \in \mathbb{R}^4, \quad \alpha = (\alpha_1, \alpha_2) \in \mathbb{R}^2, \tag{1}$$

f smooth, be a four-dimensional differential system with two parameters. Assume that $x = 0$ is an equilibrium point of the system for all α with $|\alpha| = \sqrt{\alpha_1^2 + \alpha_1^2}$ small enough, that is, $f(0, \alpha) \equiv 0$; $x = 0$ stands for $x = (0, 0, 0, 0)$ and $\alpha = 0$ for $\alpha = (0, 0)$. The system (1) can be written as

$$\dot{x} = A(\alpha) x + F(x, \alpha) \tag{2}$$

where $F(x, \alpha) = O\left(|x|^2\right)$ is a smooth function denoting Taylor series with terms of order at least 2. Assume the matrix $A(\alpha)$ has two pairs of simple complex-conjugate eigenvalues $\lambda_1, \overline{\lambda}_1, \lambda_2, \overline{\lambda}_2$,

$$\lambda_1(\alpha) = \mu_1(\alpha) + i\omega_1(\alpha), \quad \lambda_2(\alpha) = \mu_2(\alpha) + i\omega_2(\alpha)$$

---

[1] MSC (2010): 37D05, 37G05, 37G10

for all sufficiently small $|\alpha|$, where $\mu_{1,2}(\alpha)$ and $\omega_{1,2}(\alpha)$ are smooth functions of α such that $\mu_1(0) = \mu_2(0) = 0$, respectively, $\omega_1(0) = \omega_{10} > 0$ and $\omega_2(0) = \omega_{20} > 0$.

When these conditions are satisfied, the system (1) undergoes a bifurcation at $\alpha = 0$, which is known as *double-Hopf* or *Hopf-Hopf bifurcation*. Some of the classical works dealing with qualitative properties of differential systems and, particularly, bifurcations, are [1], [2], [3], [5], [9], [14] and [16]. Of the first papers studying non-degenerate double-Hopf bifurcations are [6], [7], [8] and [10]. Recent results related to double-Hopf bifurcations can be found in [4], [11], [12], [13], [15], [17].

The paper is organized as it follows. After a short introduction, in section 2 we present the system to be studied in the new conditions. We transform it into a better form, while keeping the two systems locally topologically equivalent near the origin, and present the main properties of the system in the second form. In section 3, we study the system for the new conditions and obtain new bifurcation diagrams describing the behavior of the system. Conclusive remarks end the article.

2 General analysis

The system (2) can be successively transformed in new forms by several transformations as in [9], obtaining a form in complex variables (v_1, v_2). At this stage, the system is written in polar coordinates $v_1 = r_1 e^{i\varphi_1}$, $v_2 = r_2 e^{i\varphi_2}$, which give rise to a four-dimensional system in $(r_1, r_2, \varphi_1, \varphi_2)$. Truncating higher-order terms we obtain a system in which the variables (φ_1, φ_2) are decoupled by (r_1, r_2) and satisfy $\dot{\varphi}_i = \omega_i(0)$, $i = 1, 2$. Imposing now $\rho_i = r_i^2 > 0$, $i = 1, 2$, a new two-dimensional system is obtained, called *amplitude system*, given by

$$\begin{cases} \frac{d\rho_1}{d\tau} &=& 2\rho_1 \left[\mu_1 + p_{11}\rho_1 + p_{12}\rho_2 + p_{13}\rho_1\rho_2 + s_1\rho_2^2 \right] \\ \\ \frac{d\rho_2}{d\tau} &=& 2\rho_2 \left[\mu_2 + p_{21}\rho_1 + p_{22}\rho_2 + p_{23}\rho_1\rho_2 + s_2\rho_1^2 \right] \end{cases}, \tag{3}$$

where $p_{ij} = p_{ij}(\mu)$ and $s_i = s_i(\mu)$, $i = 1, 2$, $j = 1, 2, 3$, are smooth functions depending on a parameter $\mu = (\mu_1, \mu_2)$, with $|\mu| = \sqrt{\mu_1^2 + \mu_2^2} < \varepsilon$ for some $\varepsilon > 0$ sufficiently small. In [9], using a rather complex transformation, the two terms in $\rho_1\rho_2$ from (3) are reduced to 0. We prefer to keep them but will show, as expected, they do not affect the local analysis of the system for $p_{ij}(0) \neq 0$, $i, j = 1, 2$, and $|\mu|$ sufficiently small.

Remark 2.1. *The first quadrant of the phase space, corresponding to $\rho_1 \geq 0$ and $\rho_2 \geq 0$, is invariant with respect to the flow of the system (3), because the axis*

$\rho_1 = 0$ and $\rho_2 = 0$ are invariant to the flow. Thus, the system restricted to the first quadrant is well-defined and will be studied only in this region.

The system (3) with $p_{ij}(0) \neq 0$ for $i, j = 1, 2$ has been studied in [9] and a bifurcation-based analysis was presented. In this work we present a study for the system (3) when $p_{12}(\mu) p_{21}(\mu) = 0$ for all $|\mu|$ sufficiently small, $p_{11}(0) < 0$ and $p_{22}(0) < 0$. Due to the reasons explained above, the dynamics of the system will be considered only on the first quadrant $\rho_1 \geq 0$ and $\rho_2 \geq 0$.

Consider further the transformation $(\rho_1, \rho_2) \longmapsto (\xi_1, \xi_2)$ given by

$$\xi_1 = -p_{11}(\mu) \rho_1 \text{ and } \xi_2 = -p_{22}(\mu) \rho_2. \tag{4}$$

It is well defined and nonsingular for all $|\mu|$ small enough because $p_{11}(0) \neq 0$ and $p_{22}(0) \neq 0$. By changes (4) and $t = 2\tau$, the system (3) is locally topologically equivalent near the origin for all sufficiently small $|\mu|$ to

$$\begin{cases} \frac{d\xi_1}{dt} &= \xi_1 \left(\mu_1 - \xi_1 - \theta \xi_2 + M \xi_1 \xi_2 + N \xi_2^2 \right) \\ \frac{d\xi_2}{dt} &= \xi_2 \left(\mu_2 - \delta \xi_1 - \xi_2 + S \xi_1 \xi_2 + P \xi_1^2 \right) \end{cases}, \tag{5}$$

where $\theta = \frac{p_{12}}{p_{22}}$, $M = \frac{p_{13}}{p_{11} p_{22}}$, $N = \frac{s_1}{p_{22}^2}$, $\delta = \frac{p_{21}}{p_{11}}$, $S = \frac{p_{23}}{p_{11} p_{22}}$ and $P = \frac{s_2}{p_{11}^2}$,

with $\theta = \theta(\mu)$, $\delta = \delta(\mu)$, $M = M(\mu)$, $N = N(\mu)$, $S = S(\mu)$ and $P = P(\mu)$ are smooth functions of their arguments.

The new system (5) inherits the property of being invariant with respect to the first quadrant $\xi_1 \geq 0$ and $\xi_2 \geq 0$, and the transformation (4) maps the first quadrant of the system (3) into the first quadrant of (5). Thus, the study of the new system (5) in the first quadrant is well-defined.

Remark 2.2. *The case $p_{11}(0) > 0$ and $p_{22}(0) > 0$ reduces to the previous case by a change in (3) of the form*
$\xi_1 = p_{11}\rho_1$, $\xi_2 = p_{22}\rho_2$, $t = 2\tau$ *and* $(\xi_1, \xi_2) \longmapsto (-\xi_1, -\xi_2)$.

Assume first $\theta(0) \delta(0) \neq 0$. Thus, $p_{ij}(0) \neq 0$, for all $i, j = 1, 2$. The dynamics of the system (5) is known in this case. More exactly, when $\theta(0) \delta(0) - 1 \neq 0$, $\theta(0) \delta(0) \neq 0$ and $p_{11}(0) p_{22}(0) > 0$, it has been shown in [9] that the system (5) is locally topologically equivalent near the origin for all $|\mu|$ sufficiently small to the system

$$\begin{cases} \frac{d\xi_1}{dt} &= \xi_1 \left(\mu_1 - \xi_1 - \theta(0) \xi_2 \right) \\ \frac{d\xi_2}{dt} &= \xi_2 \left(\mu_2 - \delta(0) \xi_1 - \xi_2 \right) \end{cases}. \tag{6}$$

In order to introduce the reader to specific methods of studying systems of type (5), we want to present in this section the main properties of the system (5). Bifurcation diagrams for (6) are presented in [9].

Since in what follows, the expressions of $\theta = \theta(\mu)$, $\delta = \delta(\mu)$, $M = M(\mu)$, $N = N(\mu)$, $S = S(\mu)$ and $P = P(\mu)$ are needed only at $\mu = 0$, in order to save symbols, we denote by $\theta(0) = \theta$, $\delta(0) = \delta$ and so on.

The system (5) has three equilibria $O(0,0)$, $E_1(\mu_1, 0)$ and $E_2(0, \mu_2)$ for all $|\mu|$ sufficiently small. Another equilibrium $E_3(\xi_1, \xi_2)$ exists for $|\mu|$ sufficiently small, where

$$\begin{cases} \xi_1 = \frac{-\mu_1}{\theta\delta - 1}(1 + O(|\mu|)) + \frac{\theta\mu_2}{\theta\delta - 1}(1 + O(|\mu|)) \\ \xi_2 = \frac{\delta\mu_1}{\theta\delta - 1}(1 + O(|\mu|)) + \frac{-\mu_2}{\theta\delta - 1}(1 + O(|\mu|)) \end{cases}, \tag{7}$$

provided that

$$\theta\delta - 1 \neq 0. \tag{8}$$

$O\left(|\mu|^k\right) = \sum_{i+j \geq k} c_{ij}\mu_1^i\mu_2^j$ denotes a Taylor rest of order $k \geq 1$. The existence of E_3 is based on the Implicit Function Theorem applied to the algebraic system

$$\mu_1 - \xi_1 - \theta\xi_2 + M\xi_1\xi_2 + N\xi_2^2 = 0 \text{ and } \mu_2 - \delta\xi_1 - \xi_2 + S\xi_1\xi_2 + P\xi_1^2 = 0. \tag{9}$$

The four equilibrium points are well-defined whenever their coordinates are non-negative. Two bifurcation curves determine when E_3 is born or vanishes, namely

$$T_1 = \left\{(\mu_1, \mu_2) \in \mathbb{R}^2 \mid \mu_1 = \theta\mu_2 + O\left(\mu_2^2\right), \mu_2 > 0\right\} \tag{10}$$

and

$$T_2 = \left\{(\mu_1, \mu_2) \in \mathbb{R}^2 \mid \mu_2 = \delta\mu_1 + O\left(\mu_1^2\right), \mu_1 > 0\right\}. \tag{11}$$

On T_1, E_3 coincides to $E_2(0, \mu_2)$ while on T_2 to $E_1(\mu_1, 0)$; we call E_3 *trivial* in these cases, otherwise nontrivial.

Remark 2.3. *The eigenvalues of the first three equilibria O and $E_{1,2}$ are, respectively, $\lambda_{1,2}^O = \mu_{1,2}$, $\lambda_1^{E_1} = -\mu_1$ and $\lambda_2^{E_1} = -\delta\mu_1 + \mu_2 + P\mu_1^2$, and $\lambda_1^{E_2} = -\mu_2$ and $\lambda_2^{E_2} = \mu_1 - \theta\mu_2 + N\mu_2^2$.*

The characteristic polynomial of the system (5) at an equilibrium point (ξ_1, ξ_2) of type E_3, i.e. satisfying (9), has the form $P(\lambda) = \lambda^2 - 2p\lambda + B$ where

$$p = -\frac{1}{2}(\xi_1 + \xi_2) + \frac{1}{2}(M + S)\xi_1\xi_2 \text{ and } B = -\xi_1\xi_2(\theta\delta - 1 + O(|\xi|)). \tag{12}$$

It follows immediately from (12) that the product of the eigenvalues $\lambda_{1,2}$ of E_3 satisfy $\lambda_1\lambda_2 = B$, namely

$$\lambda_1\lambda_2 = -\frac{1}{\theta\delta - 1}(-\mu_1 + \theta\mu_2)(\delta\mu_1 - \mu_2)(1 + O(|\mu|)). \tag{13}$$

Moreover, if $\lambda_{1,2}$ are of the form $\lambda_{1,2} = p \pm \sqrt{q}$ then

$$p = -\frac{1}{2\left(\theta\delta - 1\right)}\left(-\mu_1 + \theta\mu_2 + \delta\mu_1 - \mu_2\right) \text{ and } q = \frac{1}{4\left(\theta\delta - 1\right)^2}\left(a\mu_1^2 + 2b\mu_1\mu_2 + c\mu_2^2\right)$$
(14)

in their lowest terms, where $a = \left(\delta + 1\right)^2 - 4\theta\delta^2$, $b = 2\theta^2\delta^2 + \theta\delta - \theta - \delta - 1$ and $c = \left(\theta + 1\right)^2 - 4\theta^2\delta$. In general,

$$B = -\xi_1\xi_2\left(\theta\delta - 1 + m_{11}\xi_1 + \left(M - 2N\delta - S\theta\right)\xi_2 + 2MP\xi_1^2 + 4NP\xi_1\xi_2 + 2NS\xi_2^2\right),$$
(15)

where $m_{11} = S - M\delta - 2P\theta$ and

$$q = \frac{1}{4}\left(\xi_1 - \xi_2\right)^2 + \frac{1}{4}\xi_1\xi_2\left(4\theta\delta + c_{11}\xi_1 + c_{12}\xi_2 + 8MP\xi_1^2 + c_{13}\xi_1\xi_2 + 8NS\xi_2^2\right) \quad (16)$$

where $c_{11} = 2S - 2M - 4M\delta - 8P\theta$, $c_{12} = 2M - 2S - 8N\delta - 4S\theta$ and $c_{13} = 16NP + \left(M + S\right)^2$. At $\xi_2 = \xi_1$, q becomes

$$q = \theta\delta\xi_1^2 + \frac{1}{4}\left(c_{11} + c_{12}\right)\xi_1^3 + \frac{1}{4}\left(8MP + 8NS + c_{13}\right)\xi_1^4. \quad (17)$$

We state in the following a result concerning the sign of p when $\theta\delta - 1 \neq 0$, which will be used later on to show the non-existence of Hopf bifurcation at E_3.

Lemma 2.4. *If $\theta\delta - 1 \neq 0$, then $p\left(\mu_1, \mu_2\right) < 0$ whenever E_3 exists (i.e in the first quadrant) for all $|\mu|$ sufficiently small.*

Proof. If $\theta\delta - 1 > 0$, $E_3\left(\xi_1, \xi_2\right)$ is well-defined (i.e. exists in the first quadrant of the phase space) and non-trivial when $\left(\mu_1, \mu_2\right)$ lies in the region

$$R_1 = \left\{\left(\mu_1, \mu_2\right) \in \mathbb{R}^2 \mid -\mu_1 + \theta\mu_2 > 0, \delta\mu_1 - \mu_2 > 0, |\mu| < \varepsilon\right\},$$

while, if $\theta\delta - 1 < 0$, when $\left(\mu_1, \mu_2\right)$ lies in

$$R_2 = \left\{\left(\mu_1, \mu_2\right) \in \mathbb{R}^2 \mid -\mu_1 + \theta\mu_2 < 0, \delta\mu_1 - \mu_2 < 0, |\mu| < \varepsilon\right\},$$

for some $\varepsilon > 0$ small enough. Denote by H the curve $p = 0$, that is,

$$H = \left\{\left(\mu_1, \mu_2\right) \in \mathbb{R}^2, p\left(\mu_1, \mu_2\right) = 0, |\mu| < \varepsilon\right\}.$$

When $\theta\delta - 1 \neq 0$, $\theta \neq 1$ and $\delta \neq 1$, it follows that H becomes

$$H_1 = \left\{\left(\mu_1, \mu_2\right), \mu_2 = -\mu_1\frac{\delta - 1}{\theta - 1}\left(1 + O\left(\mu_1\right)\right)\right\}.$$

In finding H_1, only the linear terms in ξ_1 and ξ_2 were needed from the expression of p given in (12), thus, when $|\mu|$ is small enough, we can approximate $p = -\frac{1}{2}(\xi_1 + \xi_2)$. It follows that $p < 0$ on $R_{1,2}$ because $\xi_{1,2} > 0$ on $R_{1,2}$.

It remains to study the cases $\theta = 1$, respectively, $\delta = 1$. Assume further $\theta\delta - 1 < 0$. A similar proof can be obtained for $\theta\delta - 1 > 0$.

Consider the first case $\theta = 1$ and $\delta < 1$; $\delta \neq 0$. It follows from (12) that p is of the form $p = \frac{1}{2}\left(-\mu_1 + k_1\mu_2^2\right)$, while H becomes

$$H_2 = \left\{(\mu_1, \mu_2), \mu_1 = k_1\mu_2^2\left(1 + O\left(\mu_2\right)\right)\right\}, \tag{18}$$

where we assume $k_1 \neq 0$. One can show $H_2 \not\subseteq R_2$, thus $p(\mu)$ keeps constant sign on R_2. Indeed, assuming that there exists a point $(\mu_1, \mu_2) \in H_2 \cap R_2$, we obtain $\mu_1 = k_1\mu_2^2$, $\mu_2(1 - \mu_2 k_1) < 0$ and $\delta k_1\mu_2^2 - \mu_2 = -\mu_2(1 - \delta\mu_2 k_1) < 0$ with $|\mu|$ sufficiently small, which lead to the contradiction $\mu_2 < 0$ and $\mu_2 > 0$.

If $\delta < 0$, then $(\mu_1, 0) \in R_2$ for $\mu_1 > 0$ which leads to $p(\mu_1, 0) = -\frac{1}{2}\mu_1 < 0$, thus, $p(\mu_1, \mu_2) < 0$ on R_2.

If $0 < \delta < 1$, then any point $(\mu_1, \mu_2) \in R_2$ satisfies $\mu_2 < \mu_1 < \frac{1}{\delta}\mu_2$ which lead to $\mu_2(1 - \delta) > 0$, that is, $\mu_2 > 0$, respectively, $\mu_1 > \mu_2 > 0$. Therefore, $R_2 \subset \{\mu_1 > 0, \mu_2 > 0\}$. A point $(\mu_1, \mu_2) \in R_2$ if and only if $\mu_2 = c_0\mu_1$ where $0 < \delta < c_0 < 1$ and $\mu_1 > 0$. For such a point we have $p = \frac{1}{2}\left(-1 + k_1 c_0^2\mu_1\right)\mu_1 < 0$ for $|\mu|$ sufficiently small. It follows that $p(\mu_1, \mu_2) < 0$ on R_2.

Consider the second possibility, $\delta = 1$ and $\theta < 1$; $\theta \neq 0$. Then

$$p = \frac{1}{2}\left(-\mu_2 + k_2\mu_1^2\right)$$

by (12), while H becomes

$$H_3 = \left\{(\mu_1, \mu_2), \mu_2 = k_2\mu_1^2\left(1 + O\left(\mu_1\right)\right)\right\},$$

where we assume $k_2 \neq 0$. One shows similarly that $H_2 \not\subseteq R_2$. Indeed, if there exists a point $(\mu_1, \mu_2) \in H_2 \cap R_2$ then, $\mu_2 = k_2\mu_1^2$, $-\mu_1(1 - \theta k_2\mu_1) < 0$ and $\mu_1(1 - k_2\mu_1) < 0$. Since $|\mu|$ is sufficiently small, these lead to the contradiction $\mu_1 > 0$ and $\mu_1 < 0$. Thus, $H_2 \not\subseteq R_2$ and p keeps constant sign on R_2.

If $\theta < 0$, then $(0, \mu_2) \in R_2$ for $\mu_2 > 0$ which leads to $p(0, \mu_2) = -\frac{1}{2}\mu_2 < 0$, thus, $p(\mu_1, \mu_2) < 0$ on R_2.

If $0 < \theta < 1$, then any point $(\mu_1, \mu_2) \in R_2$ satisfies $\mu_1 < \mu_2 < \frac{1}{\theta}\mu_1$ which lead to $\mu_1(1 - \theta) > 0$, that is, $\mu_1 > 0$, respectively, $\mu_2 > \mu_1 > 0$. Therefore, $R_2 \subset \{\mu_1 > 0, \mu_2 > 0\}$. A point $(\mu_1, \mu_2) \in R_2$ if and only if $\mu_2 = b_0\mu_1$ where $1 < b_0 < \frac{1}{\theta}$ and $\mu_1 > 0$. For such a point we have $p = \frac{1}{2}\left(-b_0 + k_2\mu_1\right)\mu_1 < 0$ for $|\mu|$ sufficiently small. It follows that $p(\mu_1, \mu_2) < 0$ on R_2. $\square$

Theorem 2.5. *1) If $\theta\delta - 1 > 0$, the equilibrium E_3 is a saddle.*

2) If $\theta\delta - 1 < 0$, the equilibrium E_3 is stable (node or focus). Moreover, when $0 < \theta\delta < 1$, E_3 is a stable node whenever is nontrivial.

3) No Hopf bifurcation can occur at E_3 when $\theta\delta - 1 \neq 0$.

Proof. 1) The eigenvalues of $E_3 \left(\frac{-\mu_1 + \theta\mu_2}{\theta\delta-1}, \frac{\delta\mu_1 - \mu_2}{\theta\delta-1} \right)$ in their lowest terms satisfy (13) and $\lambda_1 + \lambda_2 = 2p$.

Assume first $\theta\delta - 1 > 0$. Then a nontrivial E_3 exists when (μ_1, μ_2) lies in the region R_1, where $\lambda_1\lambda_2 < 0$. The eigenvalues λ_1, λ_2 are real numbers on R_1 because, otherwise, if $\lambda_{1,2} = p \pm i\omega$, then $\lambda_1\lambda_2 = p^2 + \omega^2 > 0$ which contradicts $\lambda_1\lambda_2 < 0$. Thus, E_3 is a saddle point with $q > 0$. This result may also be obtained from $\lambda_1\lambda_2 = -\xi_1\xi_2 (\theta\delta - 1 + O(|\xi|))$ because $\xi_1 > 0$ and $\xi_2 > 0$ are sufficiently small for $|\mu|$ small, that is, $\theta\delta - 1 + O(|\xi|) > 0$. By (17), the result remains valid at $\xi_2 = \xi_1$.

2) In the second case $\theta\delta - 1 < 0$, a nontrivial E_3 exists on the region R_2 where $\lambda_1\lambda_2 > 0$ by (12) and $\lambda_1 + \lambda_2 = 2p < 0$ by Lemma 2.4. It follows that $\lambda_{1,2} < 0$ if $q > 0$, respectively, $Re(\lambda_{1,2}) < 0$ if $q < 0$. Thus, E_3 is stable (node or focus) whenever $\theta\delta - 1 < 0$.

Assume further $0 < \theta\delta < 1$. The equation $q = 0$ in variable μ_1 has the discriminant $\Delta = b^2 - ac$ given by

$$\Delta = 4\theta\delta (\theta\delta - 1)^3 \mu_2^2 < 0.$$

Thus, the sign of q is given by the sign of a, which is always strictly positive in this case. Indeed, if $\theta < 0$ and $\delta < 0$ then $a > 0$, while $a > (\delta - 1)^2 \geq 0$ if $\delta > 0$ and $\theta > 0$. Therefore, $q > 0$ which, in turn, implies that $\lambda_{1,2}$ are real numbers which satisfy $\lambda_1 + \lambda_2 < 0$ and $\lambda_1\lambda_2 > 0$ on R_2. It follows that $\lambda_{1,2} < 0$ and E_3 is a stable node. By (17), the result remains valid at $\xi_2 = \xi_1$ since $q = \theta\delta\xi_1^2 (1 + O(|\xi|))$ and $|\xi|$ is small enough to have $1 + O(|\xi|) > 0$.

3) From Lemma 2.4, it follows that $p \neq 0$ whenever E_3 exists and is nontrivial which, in turn, implies that the eigenvalues $\lambda_{1,2}$ cannot be purely complex of the form $\pm i\omega_0$ with $\omega_0 > 0$, thus, a Hopf bifurcation cannot occur at E_3. It implies that period orbits emerging from Hopf bifurcation do not exist around E_3. $\square$

Remark 2.6. *Since the above analysis did not use the terms with the coefficients M, N, P and S from (5), it follows that the system (5) is locally topologically equivalent near the origin for all $|\mu|$ sufficiently small to the system (6).*

3 Analysis and bifurcation diagrams at $\theta(\mu)\,\delta(\mu)=0$

3.1 The case $\theta(\mu)=0$ and $\delta(0)\neq 0$

Assume first $\theta(\mu)=0$ for all $|\mu|$ sufficiently small and $\delta(0)\overset{not}{=}\delta\neq 0$. Then $E_3(\xi_1,\xi_2)$ exists and has its coordinates in their lowest terms given $\xi_1=\mu_1+N\mu_2^2$ and $\xi_2=\mu_2-\delta\mu_1$, provided that $N(0)\overset{not}{=}N\neq 0$. The following result describes the behavior of E_3.

Theorem 3.1. *If $\theta(\mu)=0$ for all $|\mu|$ sufficiently small, $\delta(0)\neq 0$ and $N(0)\neq 0$, E_3 is an attractor (node or focus) whenever it exists for all $|\mu|$ sufficiently small.*

Proof. A nontrivial E_3 is well-defined when (μ_1,μ_2) lies in the region

$$R_3=\left\{(\mu_1,\mu_2)\in\mathbb{R}^2\mid\mu_1+N\mu_2^2>0,\mu_2-\delta\mu_1>0\right\}$$

where

$$p=-\frac{1}{2}\left(\mu_1+N\mu_2^2+\mu_2-\delta\mu_1\right)<0$$

if $\delta\neq 1$ and its eigenvalues satisfy $\lambda_1^{E_3}\lambda_2^{E_3}=\xi_1\xi_2\left(1+O(|\xi|)\right)>0$. Thus, E_3 is an attractor (node or focus) whenever $\delta\neq 1$. At $\delta=1$, p is of the form

$$p=-\frac{1}{2}\mu_2\left(1+O(|\mu|)\right)+h_1\mu_1^2\left(1+O(|\mu|)\right).$$

Assume $h_1\neq 0$. Therefore, from the Implicit Function Theorem, $p=0$ is a curve of the form

$$H_4=\left\{(\mu_1,\mu_2),\mu_2=2h_1\mu_1^2\left(1+O(\mu_1)\right)\right\}.$$

We notice that $H_4\cap R_3=\emptyset$. Indeed, assuming that there exists a point $(\mu_1,\mu_2)\in H_4\cap R_3$, then $\mu_1\left(1+O(\mu_1)\right)>0$ and $-\mu_1\left(1+O(\mu_1)\right)>0$, which is a contradiction for a fixed μ_1 with $|\mu_1|$ small enough. Thus, $p(\mu)$ keeps constant sign on R_3.

Assume first $N>0$. Then $(0,\mu_2)\in R_3$ for all $\mu_2>0$ and $p(0,\mu_2)=$ $=-\frac{1}{2}\mu_2\left(1+O(|\mu|)\right)<0$, thus, $p(\mu_1,\mu_2)<0$ for all $(\mu_1,\mu_2)\in R_3$.

If $N<0$, take a point of the form $\left(-2N\mu_2^2,\mu_2\right)\in R_3$ for all $\mu_2>0$ sufficiently small. Then $p\left(-2N\mu_2^2,\mu_2\right)=-\frac{1}{2}\mu_2\left(1+O(|\mu|)\right)<0$, thus, $p(\mu_1,\mu_2)<0$ for all $(\mu_1,\mu_2)\in R_3$.

While typically $h_1\neq 0$, when $h_1=0$ we can write p in the form

$$p=-\frac{1}{2}\mu_2\left(1+O(|\mu|)\right)+h_n\mu_1^n\left(1+O(|\mu|)\right)$$

for some $n \geq 2$ with $h_n \neq 0$. However, this does not change the proof and conclusion. $\square$

Remark 3.2. *Typically E_3 is a node when*

$$\theta(\mu)\delta(\mu) = 0$$

because $q = \frac{1}{4}(\xi_1 - \xi_2)^2 + O\left(|\xi|^3\right).$

Remark 3.3. *At $\theta(\mu) = 0$ and $\delta \neq 0$, the first three equilibria O and $E_{1,2}$ still exist with the corresponding eigenvalues*

$$\lambda_{1,2}^O = \mu_{1,2},$$

$\lambda_1^{E_1} = -\mu_1$ and $\lambda_2^{E_1} = -\delta\mu_1 + \mu_2$, respectively, $\lambda_1^{E_2} = -\mu_2$ and $\lambda_2^{E_2} = \mu_1 + N\mu_2^2$.

Two bifurcation curves determine the existence of E_3, namely T_2 (11) given by $\mu_2 = \delta\mu_1(1 + O(\mu_1))$, $\mu_1 > 0$, and

$$C_1 = \left\{(\mu_1, \mu_2) \in \mathbb{R}^2 \mid \mu_1 = -N\mu_2^2 + O\left(\mu_2^3\right)\right\}. \tag{19}$$

Different to T_2, the curve C_1 is tangent to the μ_2-axis at O. It is a parabola when $|\mu|$ is sufficiently small. Taking into account the signs of δ and N, four different bifurcation diagrams arise in this case, Figure 1. The phase portraits corresponding to the eight regions $1-8$ from the bifurcation diagrams $D1-D12$ are depicted in Figure 4.

The next table summarizes the dynamics of the four equilibria on different regions of the parametric plane $\mu_1\mu_2$ as they appear on the bifurcation diagrams for $\theta(\mu) = 0$ and $\delta(0) \neq 0$.

	1	2	3	4	5	6	7	8
O	s	r	r	r	s	a	s	s
E_1	$-$	s	s	a	a	$-$	$-$	s
E_2	a	a	s	s	$-$	$-$	s	$-$
E_3	$-$	$-$	a	$-$	$-$	$-$	a	a

Table 1: *Types of the four equilibria at $\theta(\mu)\delta(\mu) = 0$. The abbreviations are the followings: a for attractor, s for saddle and r for repeller.*
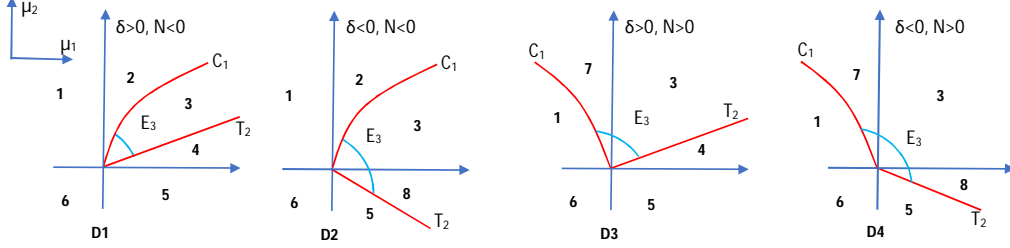
Figure 1: Bifurcation diagrams corresponding to $\theta(\mu) = 0$ and $\delta(0) \neq 0$.

3.2 The case $\theta(0) \neq 0$ and $\delta(\mu) = 0$

Secondly, assume $\theta(0) \overset{not}{=} \theta \neq 0$ and $\delta(\mu) = 0$ for all $|\mu|$ sufficiently small. Then E_3 in its lowest terms read $E_3(\xi_1^*, \xi_2^*)$ with $\xi_1^* = \mu_1 - \theta\mu_2$ and $\xi_2^* = \mu_2 + P\mu_1^2$. It is nontrivial on the region

$$R_4 = \left\{ (\mu_1, \mu_2) \mid \mu_1 - \theta\mu_2 > 0, \mu_2 + P\mu_1^2 > 0 \right\}$$

where $\lambda_1\lambda_2 = \xi_1\xi_2(1 + O(|\xi|)) > 0$ and $\lambda_1 + \lambda_2 = 2p < 0$ if $\theta \neq 1$, where p in its lowest terms is $p = -\frac{1}{2}\left(\mu_1 - \theta\mu_2 + \mu_2 + P\mu_1^2\right)$.

One shows similarly to the previous case that $p < 0$ for $\theta = 1$ as well. In conclusion, we can write the following theorem.

Theorem 3.4. *If $\delta(\mu) = 0$ for all $|\mu|$ sufficiently small, $\theta(0) \neq 0$ and $P(0) \neq 0$, E_3 is an attractor (node or focus) whenever it exists for all $|\mu|$ sufficiently small.*

The existence of E_3 is determined by T_1 (10) given by $\mu_1 = \theta\mu_2(1 + O(\mu_2))$, $\mu_2 > 0$, and a curve C_2 tangent to the μ_1–axis at O, given by

$$C_2 = \left\{ (\mu_1, \mu_2) \in \mathbb{R}^2 \mid \mu_2 = -P\mu_1^2(1 + O(\mu_1)) \right\}. \tag{20}$$

Remark 3.5. *The eigenvalues of the first three equilibria are $\lambda_{1,2}^O = \mu_{1,2}$, $\lambda_1^{E_1} = -\mu_1$ and $\lambda_2^{E_1} = \mu_2 + P\mu_1^2$, respectively, $\lambda_1^{E_2} = -\mu_2$ and $\lambda_2^{E_2} = \mu_1 - \theta\mu_2$.*

Four different bifurcation diagrams emerge in this case as well, Figure 2, depending on the signs of θ and P.

3.3 The case $\theta(\mu) = 0$ and $\delta(\mu) = 0$

Finally, assume $\theta(\mu) = \delta(\mu) = 0$. Then $E_3(\xi_1^*, \xi_2^*)$ has its coordinates $\xi_1^* = \mu_1 + N\mu_2^2$ and $\xi_2^* = \mu_2 + P\mu_1^2$, where $N \overset{def}{=} N(0) \neq 0$ and $P \overset{def}{=} P(0) \neq 0$.
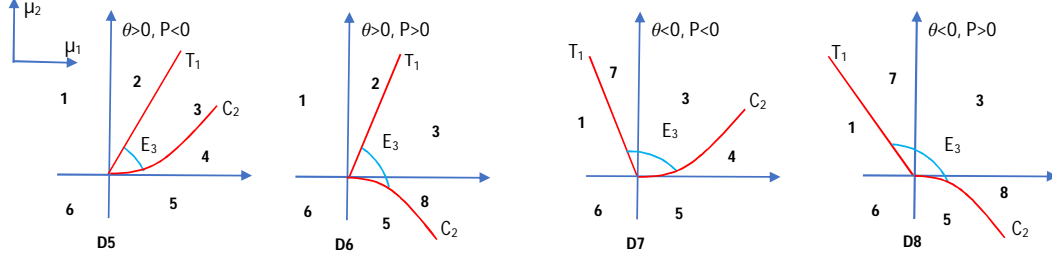
Figure 2: Bifurcation diagrams corresponding to $\delta(\mu) = 0$ and $\theta(0) \neq 0$.

E_3 exists and is nontrivial on the region stable

$$R_5 = \left\{ (\mu_1, \mu_2) \in \mathbb{R}^2 \mid \mu_1 + N\mu_2^2 > 0, \mu_2 + P\mu_1^2 > 0 \right\}$$

where

$$p = -\frac{1}{2} (\mu_1 + \mu_2) + O\left(|\mu|^2 \right).$$

It follows that $p < 0$ for $|\mu|$ sufficiently small, thus, E_3 is an attractor. Typically, E_3 is a node since $q = (\mu_1 + \mu_2)^2 \geq 0$ in its lowest terms.

Remark 3.6. *The eigenvalues of the first three equilibria are $\lambda_{1,2}^O = \mu_{1,2}$, $\lambda_1^{E_1} = -\mu_1$ and $\lambda_2^{E_1} = \mu_2 + P\mu_1^2$, respectively, $\lambda_1^{E_2} = -\mu_2$ and $\lambda_2^{E_2} = \mu_1 + N\mu_2^2$.*

Depending on the signs of N and P, four different bifurcations diagrams are obtained, Figure 3. The bifurcation diagrams depicted in Figures 1-3 corresponding to the three cases arising from $\theta(\mu)\,\delta(\mu) = 0$, are different in terms of the existing bifurcation curves in the three cases but the order of different regions in the diagrams from different cases may coincide.
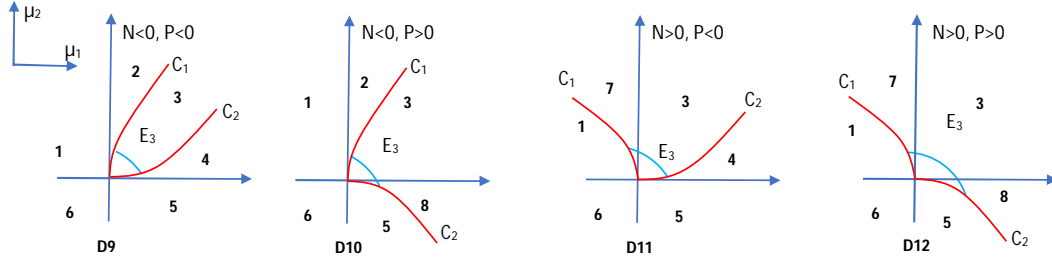

Figure 3: Bifurcation diagrams corresponding to $\theta(\mu) = 0$ and $\delta(\mu) = 0$.
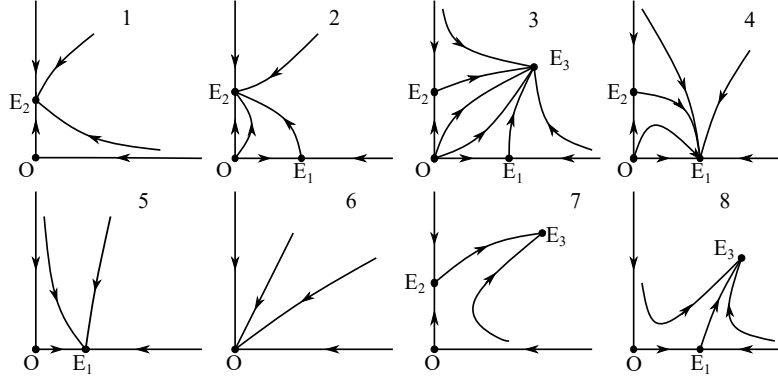
Figure 4: Phase portraits corresponding to the eight regions $1 - 8$ from the bifurcation diagrams $D1 - D12$.

4   Conclusions

We eliminated the restriction $\theta(\mu) \cdot \delta(\mu) \neq 0$ that appears in [9] in the study of the truncated normal form of double-Hopf bifurcation. In the three cases we considered, new bifurcation diagrams have been obtained which describe the behavior of the normal form in these cases. More other cases may arise by eliminating the condition $\theta(\mu) \cdot \delta(\mu) \neq 0$, which we want to approach in further studies.

5   Acknowledgements

References

[1] D. Arrowsmith, C. Place, An Introduction to Dynamical Systems, Cambridge University Press, Cambridge, 1990.

[2] H. Broer, G. Vegter, Subordinate Silnikov bifurcations near some singularities of vector fields having low codimension, Ergodic Theory Dynamical Systems 4, 509-525, 1984.

[3] S. N. Chow, C. Li and D. Wang, Normal Forms and Bifurcation of Planar Vector Fields, Cambridge University Press, Cambridge and New York, 1994.

[4] Y. Du, B. Niu, Y. Guo and J. Li, Double Hopf bifurcation induces coexistence of periodic oscillations in a diffusive Ginzburg-landau model, Physics Letters A, 383(7), 630–639, 2019.

[5] J. Guckenheimer and P. Holmes, Nonlinear Oscillations, Dynamical Systems and Bifurcations of Vector Fields, Springer, 1983.

[6] N. K. Gavrilov, Bifurcations of an equilibrium with one zero and a pair of pure imaginary roots, Methods of Qualitative Theory of Differential Equations, 1978, Gorkii State University, Gorkii.

[7] N. K. Gavrilov, Bifurcations of an equilibrium with two pairs of pure imaginary roots, Methods of Qualitative Theory of Differential Equations, Gorkii State University, Gorkii, 17-30, 1980.

[8] J. Keener, Infinite period bifurcation and global bifurcation branches, SIAM Journal Appl. Math. 41, 127-144, 1971.

[9] Y. A. Kuznetsov, Elements of Applied Bifurcation Theory (Second Edition), Appl. Math. Sci. vol. 112, Springer–Verlag, New York, 1998.

[10] W. Langford, Periodic and steady mode interactions lead to tori, SIAM Journal Appl. Math. 37, 22-48, 1979.

[11] X. Li, On the persistence of quasi-periodic invariant tori for double Hopf bifurcation of vector fields, Journal of Differential Equations, 260(10), 7320–7357, 2016.

[12] T. G. Molnar, Z. Dombovari, T. Insperger, and G. Stepan, On the analysis of the double Hopf bifurcation in machining processes via centre manifold reduction, Proceeding of the Royal Society A, 473 (2207), 2017, 1-20.

[13] V. Pa and S. Singh, Bifurcations emerging from a double Hopf bifurcation for a BWR, Progress in Nuclear Energy, 117, Article 103049, 2019.

[14] L. Perko, Differential Equations and Dynamical Systems (Third Edition), Springer Verlag, New York, 2001.

[15] G. Revel, D. M. Alonso, and J. L. Moiola, A Degenerate 2:3 Resonant Hopf–Hopf Bifurcation as Organizing Center of the Dynamics: Numerical Semiglobal Results, SIAM J. Appl. Dyn. Syst., 14(2), 1130–1164, 2015.

[16] J. Sotomayor, Generic bifurcations of dynamic systems, in M.M. Peixoto, Ed. Dynamical Systems, 561-582, 1973, New York Academic Press.

[17] Y. Zhou, Double Hopf Bifurcation of a Simply Supported Rectangular Thin Plate With Parametrically and Externally Excitations, Journal of space exploration, 6(3), 1-16, 2017.

Gheorghe Ţigan and Emanuel Cismaş
Department of Mathematics,
Politehnica University of Timisoara,
Victoriei Square 2, 300006 - Timisoara, ROMANIA
E-mail: gheorghe.tigan@upt.ro
E-mail: emanuel.cismas@upt.ro

Stelian Mihalaş and Oana Brandibur
Department of Mathematics
Faculty of Mathematics and Informatics,
West University of Timisoara,
V.Parvan 4, 300223 - Timisoara, ROMANIA
E-mail: stelian.mihalas@e-uvt.ro
E-mail: oana.brandibur92@e-uvt.ro

APPROXIMATE SOLUTIONS FOR RICCATI DIFFERENTIAL EQUATION OF FRACTIONAL ORDER USING THE LEAST SQUARES DIFFERENTIAL QUADRATURE METHOD

Bogdan CĂRUNTU, Constantin BOTA,
Mădălina Sofia PAŞCA, Marioara LĂPĂDAT

Abstract

In the present paper we employ a recently introduced approximation method, namely the Least Squares Differential Quadrature Method (LSDQM), in order to compute analytical approximate polynomial solutions for several quadratic Riccati differential equation of fractional order. [1]

Keywords and phrases: *Riccati differential equation of fractional order, Least squares differential quadrature method (LSDQM)*

1 Introduction

In the last decades, fractional differential equations were the focus of intense research due to their importance in many real life applications like viscoelasticity ([1]), chemical engineering ([2]),fluid mechanics ([5]) or signal processing ([4]). In this paper we will consider the following class of Riccati differential equations of fractional order:

$$D^\alpha y(t) - A(t)y^2(t) - B(t)y(t) = f(t), \ \ 0 < \alpha \le 1, \ \ t \in [0,1], \tag{1}$$

together with an initial condition of the type:

$$y(0) = k, \tag{2}$$

where $A(t)$, $B(t)$ and $C(t)$ are given real functions, k is a given real constant and $D^\alpha y(t)$ denotes Caputo's fractional derivative of order α:

$$D^\alpha y(t) = \frac{1}{\Gamma(n-\alpha)} \cdot \int_0^t (t-\zeta)^{-(\alpha-n+1)} \cdot y^{(n)}(\zeta)d\zeta, \qquad n-1 < \alpha \le n \tag{3}$$

---

[1]MSC (2010): 34K28, 45L05

The Riccati differential equation of fractional order has been studied both numerically and analytically in numerous articles. Among the methods used to solve this equation we mention: Jacobi collocation method (JCM)([3]), Variational iteration method (VIM)([6]), modified homotopy perturbation method ($MHPM$) ([7]), optimal homotopy asymptotic method ($OHAM$) ([8]), Polynomial Least Squares Method ($PLSM$) ([9]).

2 The Least Squares Differential Quadrature Method (LSDQM)

The Least Squares Differential Quadrature Method (LSDQM) ([10]) allow us to compute approximate analytical polynomial solutions for fractional differential Riccati equations of the type (1). In order to obtain an approximate analytical polynomial solution for the equation (1), we will consider a numerical meshing of the interval $I = [0, 1]$ by means of a partition Δ_M consisting of $M + 1$ equidistant points:

$\Delta_M : \ 0 = t_0 < t_1 < t_2 < \cdots < t_{M-1} < t_M = 1$.

To the equation (1) we attach the following operator D:

$$D(y(t)) = D^\alpha y(t) - A(t)y^2(t) - B(t)y(t) - f(t). \tag{4}$$

We denote by $\tilde{y}(t)$ an approximate solution of the equation (1). By replacing in D the exact solution $y(t)$ with this approximate solution we obtain the *reminder* $\mathcal{R}$:

$$\mathcal{R}(t, \tilde{y}(t)) = D(\tilde{y}(t)), \qquad t \in [0, 1]. \tag{5}$$

Definition 1. *We call an ϵ-**approximate** solution of the problem (1 - 2) related to the partition Δ_M an approximate polynomial solution which satisfies the following relations:*

$$\mathcal{R}(t_i, \tilde{y}(t_i)) < \epsilon, \qquad i = \overline{0, M}, \tag{6}$$

$$\tilde{y}(0) = k. \tag{7}$$

Definition 2. *We consider the sequence of polynomials:*

$$P_N(t) = \sum_{k=0}^{N} d_k t^k, \qquad d_k \in \mathbb{R}, \qquad k = \overline{0, N}. \tag{8}$$

*We call the sequence of polynomials $P_N(t)$ **convergent** to the solution of the problem (1 - 2) if:*

$$\lim_{N \to \infty} D(P_N(t)) = 0. \tag{9}$$

We will compute ϵ - approximate polynomial solutions of the type:

$$T_N(t) = \sum_{k=0}^{N} \tilde{d}_k t^k, \tag{10}$$

with the initial condition: $T_N(0) = k$.

The constants $\tilde{d}_k$ are calculated by taking the following steps:

- From the initial condition we obtain $\tilde{d}_0$ as function of $\tilde{d}_1, \tilde{d}_2 \cdots \tilde{d}_N$ and replace them in the expression of $T_N(t)$ (which from now on will be a function of $\tilde{d}_1, \tilde{d}_2, \cdots, \tilde{d}_N$ only).

- We attach to the problem (1 - 2) the functional:

$$\mathcal{J}(\tilde{d}_1, \tilde{d}_2, \cdots, \tilde{d}_N) = \sum_{i=0}^{M} \mathcal{R}^2(t_i, T_N(t_i)). \tag{11}$$

- By minimizing the functional (11) we obtain the coefficients $\tilde{d}_1, \tilde{d}_2 \cdots \tilde{d}_N$.

- We replace the coefficients $\tilde{d}_1, \tilde{d}_2 \cdots \tilde{d}_N$.in the expression (10) and denote by $T_N^0(t) = \sum_{k=0}^{N} \tilde{d}_k t^k$, the analytical approximate polynomial solutions by LSDQM of the problem (1 - 2).

The following convergence theorem is satisfied:

Theorem 1. *The sequence of polynomials $T_N^0(t)$ satisfies the relations:*

$$\lim_{N \to \infty} \mathcal{R}^2(t_i, T_N^0(t_i)) = 0, \qquad i = \overline{0, M}. \tag{12}$$

Proof. Let $y(t)$ be an exact solution of the problem (1 - 2), which means from hypothesis that there exist a sequence of polynomials $P_N(t)$ with $P_N(t) = \sum_{k=0}^{N} d_k t^k$, $d_k \in \mathbb{R}, \quad k = \overline{0, N}$ converging to $y(t)$: $\quad \lim_{N \to \infty} P_N(t) = y(t), \quad \forall t \in I$.

We know that

$$\sum_{i=0}^{M} \mathcal{R}^2(t_i, T_N^0(t_i)) \leq \sum_{i=0}^{M} \mathcal{R}^2(t_i, P_N(t_i)),$$

hence

$$\lim_{N \to \infty} (\sum_{i=0}^{M} \mathcal{R}^2(t_i, T_N^0(t_i))) \leq \lim_{N \to \infty} (\sum_{i=0}^{M} \mathcal{R}^2(t_i, P_N(t_i))).$$

We conclude that $\quad \lim_{N \to \infty} \mathcal{R}^2(t_i, T_N^0(t_i)) = 0, \qquad i = \overline{0, M}.$ $\qquad \square$

In that way we obtain the polynomial $T_N^0(t_i)$ which approximates the solution of the problem (1 - 2).

3   Applications

Application 1

We consider $A(t) = t^3$, $B(t) = -2t^4$, $f(t) = t^5 + 1$ and $k = 0$, obtaining the problem ([3]):

$$\begin{cases} D^\alpha y(t) - t^3 y^2(t) + 2t^4 y(t) = t^5 + 1 \\ y(0) = 0, \end{cases} \quad for \ t \in \ [0,1]; \quad 0 < \alpha \le 1 \tag{13}$$

Case $\alpha = 1$:

The exact solution of this problem for integer order $\alpha = 1$, is $y(t) = t$ ([3]).

Using the LSDQ method we computed a solution of the type (10):

$$P_1(t) = d_0 + d_1 \cdot t.$$

Taking into account the initial condition $P_1(0) = 0$, we obtain $d_0 = 0$, and the approximation becomes: $P_1(t) = d_1 \cdot t$.
The corresponding remainder (5) in this case is :

$$\mathcal{R}(t, P_1(t)) = -d_1^2 t^5 + 2d_1 t^5 + d_1 - t^5 - 1$$

and the functional$\mathcal{J}$ (11) is:

$$\mathcal{J}(\tilde{d}_1) = \tilde{d}_1^4 - 6\tilde{d}_1^3 + 13\tilde{d}_1^2 - 12\tilde{d}_1 + 4.$$

We will find the value of $\tilde{d}_1$ by minimizing this functional. In order to do that we will first find the critical points as the solutions of the equation: $\mathcal{J}'(\tilde{d}_1) = 0$ and a simple computation shows that the minimum value is $\tilde{d}_1 = 1$. Thus we are able to obtain the exact solution of the problem: $\tilde{y}(t) = t$.

Case $0 < \alpha \le 1$:

Using the steps outlined in the previous section, we computed the following approximate solutions by LSDQ Method of the problem (12) :
- first order polynomial for $\alpha = 0.9$ $\tilde{y}(t) = 0.953415t$;
- first order polynomial for $\alpha = 0.8$ $\tilde{y}(t) = 0.923537t$;

- first order polynomial for $\alpha = 0.7$ $\tilde{y}(t) = 0.905487t$;

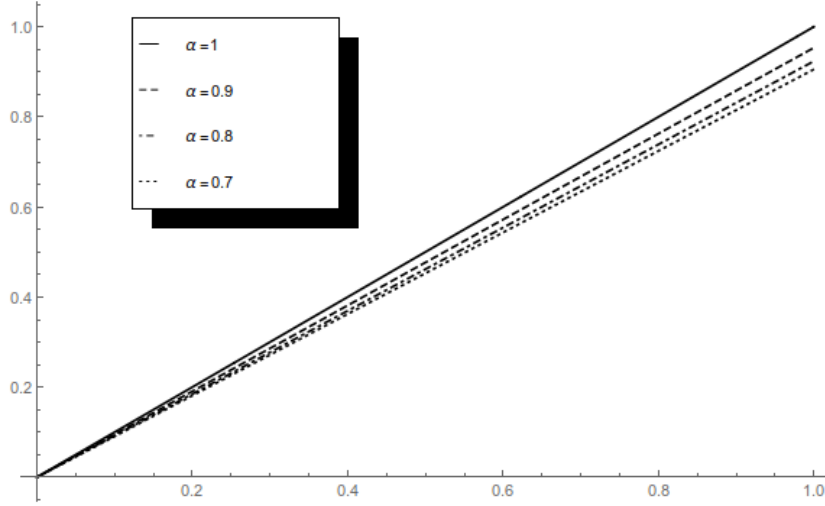These approximate analytical solutions by the Least Squares Differential Quadrature Method are presented the Fig. 1:

Figure 1: The LSDQM solution for Application 1 with $\alpha \in (0,1]$

Application 2

Choosing $A(t) = -1$, $B(t) = 0$, $f(t) = 1$, and $k = 0$, the problem (1-2) becomes ([3]):

$$\begin{cases} D^\alpha y(t) + y^2(t) = 1 \\ y(0) = 0, \end{cases} \qquad for\ t \in [0,1]; \quad 0 < \alpha \leq 1 \qquad (14)$$

The exact solution of this problem **for integer order** $\alpha = 1$ is given as: $y(t) = \dfrac{e^{2t} - 1}{e^{2t} + 1}$ ([3]). Following the LSDQM steps presented in the previous section, we compute a fifth degree polynomial approximate solution of the type (10):

$$P_5(t) = d_0 + d_1 \cdot t + d_2 \cdot t^2 + d_3 \cdot t^3 + d_4 \cdot t^4 + d_5 \cdot t^5.$$

Using the boundary condition we obtain $d_0 = 0$ and the remainder operator is:

$$\mathcal{R}(t, P_5(t)) = \left(d_1 t + d_2 t^2 + d_3 t^3 + d_4 t^4 + d_5 t^5\right)^2 + d_1 + 2d_2 t + 3d_3 t^2 + 4d_4 t^3 + 5d_5 t^4 - 1.$$

We consider the partition Δ_{100}: $0 = t_0 < t_1 < \cdots < t_{100} = 1$ with equidistant points $t_i = t_{i-1} + h$, where $h = 0.01$.

Next we attach to the problem (14) the functional

$$\mathcal{J}(\tilde{d}_1, \tilde{d}_2, \tilde{d}_3, \tilde{d}_4, \tilde{d}_5) = \sum_{i=0}^{100} \mathcal{R}^2(t_i, P_5(t_i))$$

(too long to be included here).

By minimizing this functional we find $\tilde{d}_1, \tilde{d}_2, \tilde{d}_3, \tilde{d}_4, \tilde{d}_5$. Replacing this values in the last expression of $P_5(x)$ we obtain the analytical approximate solution of the problem (14) by LSDQM as:

$$\tilde{y}(t) = -0.0169741t^5 + 0.187308t^4 - 0.42752t^3 + 0.0201815t^2 + 0.998592t.$$

We also solved the problem using a polynomial approximation of seventh degree and following the steps described above, we obtain the analytical approximate solution:

$$\tilde{y}(t) = 0.0218375t^7 - 0.122277t^6 + 0.226193t^5 - 0.0385853t^4 -$$
$$- 0.324675t^3 - 0.000934549t^2 + 1.00004t.$$

Making an approximation with a polynomial of ninth degree we obtain the following analytical approximate solution:

$$\tilde{y}(t) = -0.0106499t^9 + 0.0567198t^8 - 0.103159t^7 + 0.0253077t^6 + 0.125355t^5 +$$
$$+ 0.00150336t^4 - 0.333491t^3 + 7.886787623886357 \times 10^{-6}t^2 + 1.0t$$

In Table 1 we present the comparison between the solutions obtained by Least Squares Differential Quadrature Method ($LSDQM$) and the solutions obtained by H. Singh and H. Sirvastava in ([3]) using the Jacobi collocation method (JCM), by B. Batiha et all in ([6]) using the Variational iteration method (VIM) and by Z. Odibat using a modified homotopy perturbation method ($MHPM$).

In the Figure 2 we present the error obtained for the approximation with nine degree polynomial for the solution $\tilde{y}(t)$ for $t \in [0, 1]$.

Using LSDQ Method we computed the following approximate solution for: $0 < \alpha \le 1$, the approximate solution being of polynomial type of nine degree:

- for $\alpha = 0.9$, $\tilde{y}(t) = 22.895t^9 - 113.364t^8 + 237.882t^7 - 275.595t^6 + 192.552t^5 - 83.2439t^4 + 22.0942t^3 - 4.00524t^2 + 1.53857t$

- for $\alpha = 0.8$, $\tilde{y}(t) = 29.9235t^9 - 161.836t^8 + 371.86t^7 - 473.01t^6 + 363.877t^5 - 173.923t^4 + 51.5883t^3 - 10.0314t^2 + 2.29541t$

Table 1: Comparison of absolute error from JCM, VIM, MHPM and LSDQ Method for $\alpha = 1$

t	JCM	VIM	MHPM	$LSDQ5^{th}$deg	$LSDQ7^{nd}$deg	$LSDQ9^{th}$deg
0.1	$4.57 \cdot 10^{-9}$	$5 \cdot 10^{-11}$	0	$1.59 \cdot 10^{-5}$	$1.44 \cdot 10^{-7}$	$1.23 \cdot 10^{-9}$
0.2	$9.74 \cdot 10^{-10}$	$4.39 \cdot 10^{-9}$	0	$2.43 \cdot 10^{-5}$	$1.71 \cdot 10^{-7}$	$2.14 \cdot 10^{-10}$
0.3	$3.71 \cdot 10^{-9}$	$1.56 \cdot 10^{-7}$	$1.10 \cdot 10^{-6}$	$1.41 \cdot 10^{-5}$	$5.6 \cdot 10^{-7}$	$3.78 \cdot 10^{-10}$
0.4	$1.29 \cdot 10^{-9}$	$1.97 \cdot 10^{-6}$	$5.01 \cdot 10^{-6}$	$2.32 \cdot 10^{-5}$	$2.55 \cdot 10^{-8}$	$3.52 \cdot 10^{-9}$
0.5	$1.93 \cdot 10^{-9}$	$1.38 \cdot 10^{-5}$	$3.91 \cdot 10^{-5}$	$3.95 \cdot 10^{-5}$	$2.55 \cdot 10^{-7}$	$1.71 \cdot 10^{-9}$
0.6	$2.74 \cdot 10^{-9}$	$6.61 \cdot 10^{-5}$	$1.93 \cdot 10^{-4}$	$1.82 \cdot 10^{-5}$	$1.80 \cdot 10^{-7}$	$1.10 \cdot 10^{-9}$
0.7	$4.32 \cdot 10^{-9}$	$2.43 \cdot 10^{-4}$	$7.37 \cdot 10^{-4}$	$1.58 \cdot 10^{-5}$	$4.27 \cdot 10^{-7}$	$4.08 \cdot 10^{-9}$
0.8	$2.43 \cdot 10^{-9}$	$7.35 \cdot 10^{-4}$	$2.33 \cdot 10^{-3}$	$2.18 \cdot 10^{-5}$	$1.14 \cdot 10^{-8}$	$2.38 \cdot 10^{-9}$
0.9	$3.59 \cdot 10^{-10}$	$1.91 \cdot 10^{-3}$	$6.37 \cdot 10^{36}$	$1.05 \cdot 10^{-5}$	$8.92 \cdot 10^{-8}$	$1.81 \cdot 10^{-9}$
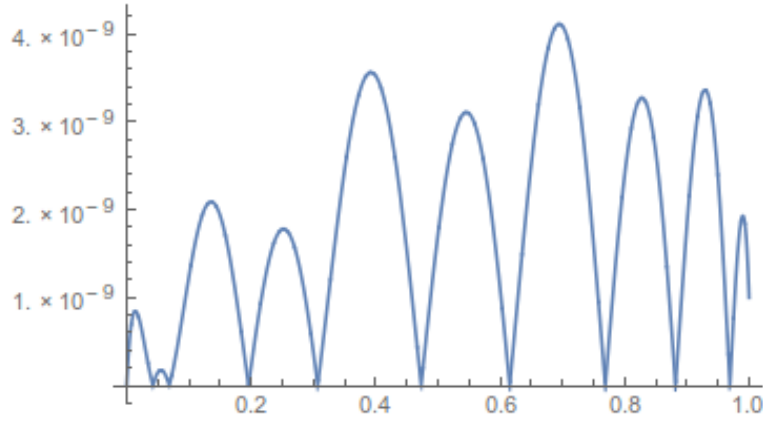
Figure 2: The absolute error corresponding to $\tilde{y}(t)$ for the case $\alpha = 1$ in Eq (14)

- for $\alpha = 0.7$, $\tilde{y}(t) = 19.9911t^9 - 147.74t^8 + 423.678t^7 - 637.806t^6 + 560.682t^5 - 298.769t^4 + 96.9138t^3 - 19.5875t^2 + 3.36745t$

In the Figure 3 we have plotted the approximate solutions for $\alpha = 0.7, 0.8, 0.9$ and 1.

Application 3

Our third application is the following Riccati differential equation of fractional order with initial condition:

$$\begin{cases} D^\alpha y(t) + y^2(t) - 2y(t) = 1 \\ y(0) = 0, \end{cases} \quad for \ t \in \ [0,1]; \quad 0 < \alpha \leq 1 \quad (15)$$
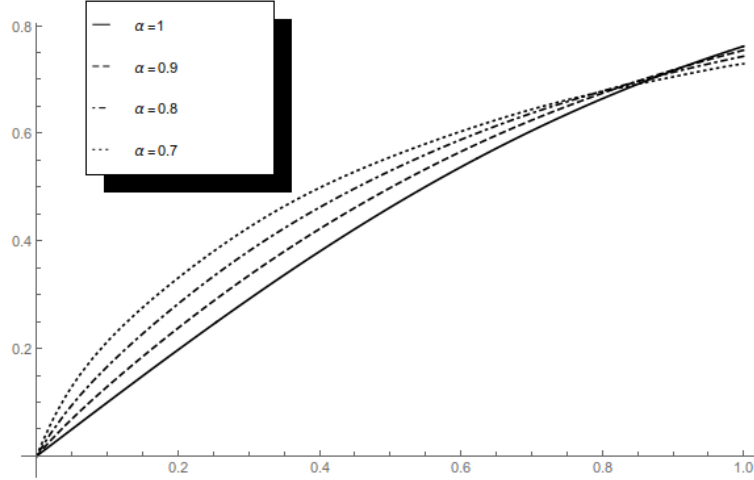
Figure 3: The LSDQM solution for Application 2 with $\alpha \in (0, 1]$

For $\alpha = 1$ the exact solution of the problem is ([3]):

$$y(t) = \sqrt{2} \tanh\left(\sqrt{2}t + \frac{1}{2}\log\left(\frac{\sqrt{2} - 1}{1 + \sqrt{2}}\right)\right) + 1.$$

In this case (equation (15) for $\alpha = 1$), by using LSDQM we computed the following approximate solution:
$\tilde{y}(t) = 0.225567t^9 - 1.37073t^8 + 2.94539t^7 - 2.49398t^6 + 0.64701t^5 - 0.640656t^4 + 0.380312t^3 + 0.996486t^2 + 1.0001t$.
Figure 4 presents the absolute error corresponding to our approximate solution $\tilde{y}(t)$ as the difference in absolute value between the approximate solution and the exact solution for the case $\alpha = 1$.

In Table 2 we present the comparison between the Least Squares Differential Quadrature Method ($LSDQM$) solution and the solutions obtained by H. Singh and H. Sirvastava in ([3]) using Jacobi collocation method (JCM), B. Batiha et all in ([6]) using Variational iteration method (VIM) and F. Mabood et all in ([8]) using optimal homotopy asymptotic method ($OHAM$).

Using LSDQ Method we computed the following approximate solution:

- for $\alpha = 0.9$, $\tilde{y}(t) = 21.6719t^9 - 106.446t^8 + 220.499t^7 - 251.061t^6 + 172.905t^5 - 75.3353t^4 + 19.9157t^3 - 1.93746t^2 + 1.5514t$

- for $\alpha = 0.8$, $\tilde{y}(t) = 38.1977t^9 - 195.105t^8 + 424.005t^7 - 512.343t^6 + 377.939t^5 - 174.904t^4 + 48.2756t^3 - 6.6356t^2 + 2.3775t$
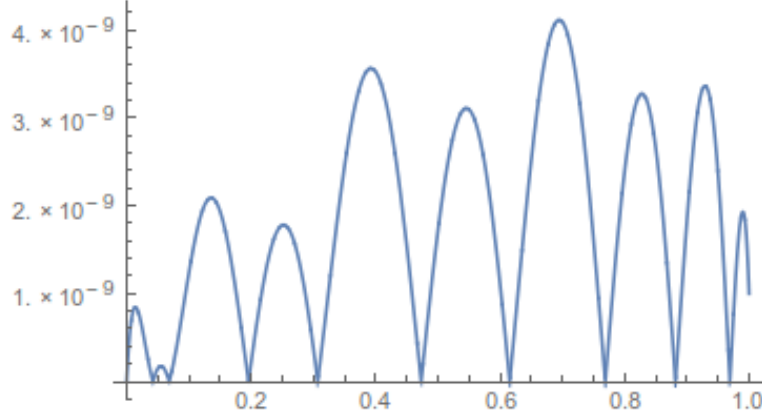
Figure 4: The absolute error corresponding to $\tilde{y}(t)$ for the case $\alpha = 1$ in Eq (15)

Table 2: Comparison of absolute error from JCM, VIM, OHAM and LSDQ Method for $\alpha = 1$

t	JCM	VIM	$OHAM$	$LSDQM$
0.1	$7.45 \cdot 10^{-7}$	$1.98 \cdot 10^{-8}$	$3.2 \cdot 10^{-5}$	$6.13 \cdot 10^{-8}$
0.2	$8.51 \cdot 10^{-7}$	$1.03 \cdot 10^{-6}$	$2.90 \cdot 10^{-4}$	$1.37 \cdot 10^{-6}$
0.3	$9.30 \cdot 10^{-7}$	$8.85 \cdot 10^{-6}$	$1.10 \cdot 10^{-3}$	$1.23 \cdot 10^{-7}$
0.4	$1.08 \cdot 10^{-6}$	$3.33 \cdot 10^{-51}$	$2.50 \cdot 10^{-3}0$	$4.75 \cdot 10^{-7}$
0.5	$1.14 \cdot 10^{-6}$	$7.26 \cdot 10^{-5}$	$4.40 \cdot 10^{-3}0$	$1.68 \cdot 10^{-6}$
0.6	$1.14 \cdot 10^{-6}$	$9.96 \cdot 10^{-5}$	$5.50 \cdot 10^{-3}0$	$5.63 \cdot 10^{-7}$
0.7	$1.21 \cdot 10^{-6}$	$8.84 \cdot 10^{-5}$	$5.51 \cdot 10^{-3}$	$2.90 \cdot 10^{-7}$
0.8	$1.04 \cdot 10^{-6}$	$1.54 \cdot 10^{-5}$	$3.80 \cdot 10^{-3}$	$1.48 \cdot 10^{-6}$
0.9	$1.13 \cdot 10^{-6}$	$4.95 \cdot 10^{-4}$	$3.20 \cdot 10^{-3}$	$2.91 \cdot 10^{-7}$
1	$4.84 \cdot 10^{-7}$	$3.47 \cdot 10^{-3}$	$3.40 \cdot 10^{-3}$	$8.37 \cdot 10^{-7}$

- for $\alpha = 0.7$, $\tilde{y}(t) = 32.9146t^9 - 197.034t^8 + 495.78t^7 - 685.108t^6 + 567.588t^5 - 286.392t^4 + 83.9888t^3 - 13.5326t^2 + 3.61622t$

    In the Figure 4 we have plotted the approximate solution for different value of $\alpha = 0.7, 0.8, 0.9$ and 1.
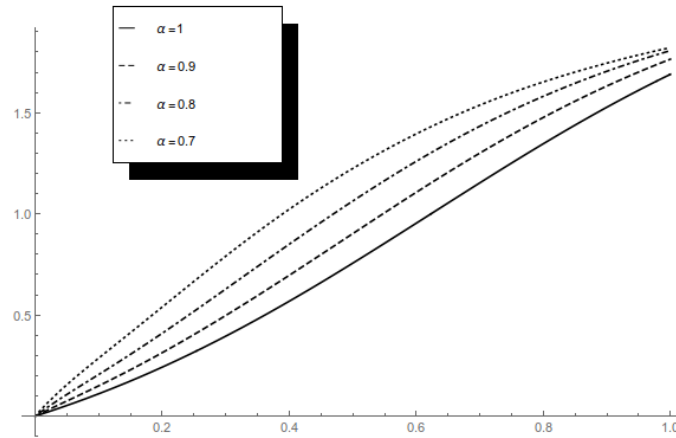
Figure 5: The LSDQM solution for Application 3 with $\alpha \in (0, 1]$

4 Conclusions

In the present paper we obtained analytical approximate solutions for several Riccati differential equations of fractional order using the Least Squares Differential Quadrature Method. Using the LSDQM one obtains the analytical solution of the equations, not only numerical solutions, fact which demonstrates the usefulness of the (LSDQM). The applications presented clearly illustrate good concordance between the LSDQM solutions and other approximate solutions.

References

[1] R. L. Bagley, P.J. Torvik, *A theoretical basis for the application of fractional calculus to viscoelasticity*, J. Rheol. 27 (1983) 201–210.

[2] H. Singh, *A new numerical algorithm for fractional model of bloch equation in nuclear magnetic resonance*, Alex. Eng. J. 55 (2016) 2863–2869.

[3] H. Singh, H.M. Srivastava, *Jacobi collocation method for the approximate solution of some fractional-order Riccati differential equations withvariable coefficients*, Physica A 523 (2019) 1130–1149.

[4] R. Panda, M. Dash, *Fractional generalized splines and signal processing*, Signal Process. 86 (2006) 2340.

[5] H. Singh, *A new stable algorithm for fractional Navier–Stokes equation in polar coordinate*, Int. J. Appl. Comp. Math. (2017) http://dx.doi.org/10.1007/s40819-017-0323-7.

[6] B. Batiha, M.S.M. Noorani, I. Hashim, *Application of variational iteration method to a general Riccati equation*, Int. Math. Forum 2 (56) (2007) 2759–2770.

[7] Z. Odibat, S. Momani, *Modified homotopy perturbation method: Application to quadratic Riccati differential equation of fractional order*, Chaos Solitons Fractals 36 (1) (2008) 167–174.

[8] F. Mabood, A.I. Ismail, I. Hashim, *Application of optimal homotopy asymptotic method for the approximate solution of Riccati equation*, Sains Malays. 42 (6) (2013) 863–867.

[9] C. Bota, B. Caruntu, *Analytical approximate solutions for quadratic Riccati differential equation of fractional order using the Polynomial Least Squares Method*, Chaos, Solitons and Fractals 102 (2017) 339–345

[10] B. Caruntu, C. Bota, M. Lapadat and M. Pasca *Polynomial Least Squares Method for Fractional Lane–Emden Equations*, Symmetry 2019, 11(4), 479; https://doi.org/10.3390/sym11040479 .

Bogdan Căruntu, Constantin Bota,
Mădălina Paşca, Marioara Lăpădat
Department of Mathematics,
Politehnica University of Timişoara,
Piaţa Victoriei 2, 300006 Timişoara, ROMANIA
E-mail: bogdan.caruntu@upt.ro
E-mail: constantin.bota@upt.ro
E-mail: madalina.pasca@upt.ro
E-mail: maria.lapadat@upt.ro

Mădălina Paşca
West University Timişoara,
V.Parvan 4, 300223 Timişoara, ROMANIA
E-mail: madalina.pasca79@e-uvt.ro

STATISTICAL ANALYSIS OF MINIMUM OIL CIRCUIT BREAKER FAILURES

Dragan STEVANOVIĆ, Aleksandar JANJIĆ, Dragan TASIĆ

Abstract

In this paper, remaining useful life (RUL) of circuit breakers (CB) has been analyzed, based on statistical data gathered during CB's maintenance. Using statistical data of 427 CBs gathered in past 10 years, Weibull probability distribution of contact resistance for breakers on both overhead and underground feeders and voltage levels of 35 kV and 10 kV is determined. With this methodology CB's condition can be observed by using real field data which are collected regullary during power station revision. [1]

Keywords and phrases: *circuit breaker, remaining useful life, voltage drop, Weibull distribution*

1 Introduction

Circuit breaker is a device used for switching feeder power supply in any working mode (normal load, no load, short circuit current...), and therefore represents the vital element of power system operation. CB failure threatens work of other equipment, which directly affects reliability of whole substation. This makes good reason of analyzing CB working behavior and its RUL.

To determine economic effects of maintenance, overhaul or CB removal [1], [2], assessment of circuit breakers remaining useful life (RUL) must be done [3], [4]. Remaining useful life is the lifetime from current time to the time that the device fails [1]. It is random variable which depends on various factors (device age, working conditions, and level of maintenance) [5]. If the failure time of the population follows the probability density function (PDF) f(t), then the population mean time to failure (MTTF) can be calculated by (1):

$$MTTF = \int_0^\infty t f(t) dt = \int_0^\infty R(t) \tag{1}$$

---

[1]PACS: 84.70.+p

$R(t)$ is the survival function at t. Let define X_t as the random variable of the RUL at time t, then the probability density function (PDF) of X_t conditional on Y_t is denoted as $f(x_t/Y_t)$ where Y_t is the history of operational information up to t. If Y_t is not available then the estimation of $f\ (x_{t/}\,Y_t)$ is:

$$f(x_t/Y_t) = f(x_t) = \frac{f(t + x_t)}{R(t)} \tag{2}$$

where $f(t + xt)$ is the PDF of the life at $t + x_t$

CB's reliability analysis depends of type of available data, which can be: contact resistance, commutation noise, erosion resistance, ultrasound detectors, transient earth voltage, infrared thermo scanning, CB control circuit data and collected data of CB faults. Depending of collected data type, RUL can be assessed with: knowledge-based models (fuzzy method); life expectancy models (statistical method [5] – [9]); artificial neural networks and physical models [4].

Utilities, grid operators and industrial power consumers are facing unprecedented challenges. With increasingly aging infrastructure combined with cost-cutting pressures to operate into today's competitive environment, prioritizing investment has never been so important.

Because of importance of reliability, some companies are started to use software, algorithms and analysis techniques for reliability management services to provide substation owners with the right insights to make optimal investments to improve system performance.

2 CB Ageing Process

The main causes of CB deterioration are the age, the number of operations under normal and fault conditions and the operational conditions like the temperature and contaminants content.

Measuring the contact resistance is usually done by using the principles of Ohm's law. Since the interrupting chamber is a closed container, we have only access to the entry and exit conductors; the measured R between these two points would be the sum of all the contact resistances found in series. According to the IEC 60694 [10], article 6.4.1, the current value to use should be the closest to the nominal current the interrupting chamber is designed for. If it is impossible to do so, lower currents can be used but not less than 50 A to eliminate the galvanic effect that might affect the readings.

2.1 Data collecting

Analysis in this paper covers 42 35/10 kV substations of Serbian state owned utility "EPS Distribucija" and 427 circuit breakers, mounted on 10kV and 35kV feeders. Measurement of static contact resistance presented by the voltage drop on contacts is collected in past 10 year period (2007 – 2017), where voltage drop was measured every two years.

Other data regarding to circuit breakers that are collected are: voltage level, feeder type, manufacturing year, number of fault trips, number of short circuit current trips, number of customers, and annual consumption.

Depending on CB's nominal current and nominal voltage allowed voltage drop goes from 3.5 mV up to 14 mV [11]. Analyzed CBs have following maximal voltage drop values: 35 kV CB's: 3.5 – 7 mV; 10 kV CB's: 7 – 14 mV.

Manufacturer manual [11] states that CB must be completely overhauled after: 10-12 years of service, or 5000 operations, or 6 short-circuit currents breaking.

Measurement has been done with DC current of I = 100A, measuring voltage drop on every CB's pole. Figure 1 shows voltage drop distribution among all currently available data, with values divided into 4 categories depending of voltage drop level.

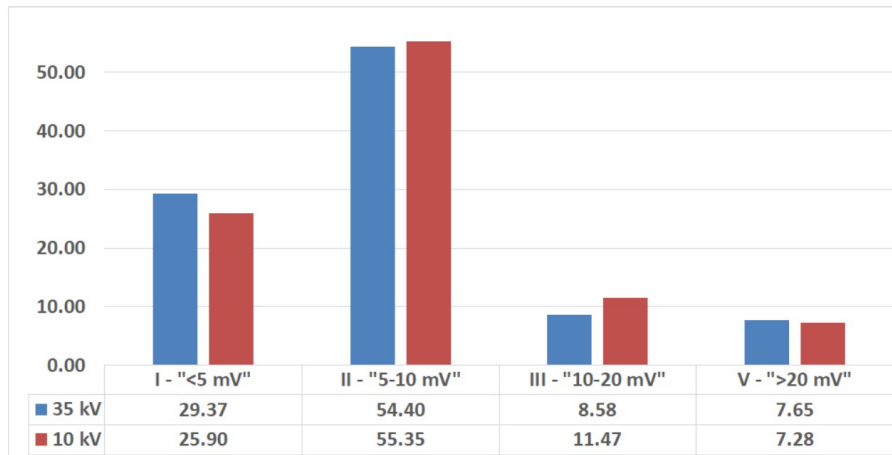|	I - "<5 mV"	II - "5-10 mV"	III - "10-20 mV"	V - ">20 mV"
35 kV	29.37	54.40	8.58	7.65
10 kV	25.90	55.35	11.47	7.28

Figure 1: Voltage drop distribution on analyzed circuit breakers

2.2 Data analyzing

In the first step, state of every CB is determined, according to its voltage drop value. CBs with voltage drop value beyond permissible are set in "failed" state (F), and those which still have voltage drop value below allowed are in "suspension" state (S). For failed CB's, the precise year of reaching that condition is defined. Such data are divided into following categories:

1. Circuit breakers on 35 kV feeders

2. Circuit breakers on 10 kV feeders

3. Circuit breakers on overhead feeders

4. Circuit breakers on underground feeders

5. All circuit breakers

From manufacturers manual [11] allowed voltage drop values are dependent on CB's rated voltage and rated current, and manufacturer allows them to surpass the permissible value for 25%. For that reason, CB's are also analyzed for two different criterions:

1. Maximal allowed voltage drop value is as in manufacturers table,

2. Maximal allowed voltage drop is 25% greater than recommended values.

That way, impact on CB's condition for both criterions is taken into account.

Obtained correlation coefficients in the curve fitting process are showing the great correlation to the Weibull probability distribution. The closer the value of Rho is to 1, the better the linear fit. Values of Rho are presented in Table I.

Correlation Coefficient [12] is a measure of how well the linear regression model (the probability line) fits the data. In the case of life data analysis, it is a measure of the strength of the linear relation (correlation) between the median ranks and the data. The population correlation coefficient is defined as follows:

$$\rho = \frac{\sigma_{xy}}{\sigma_x \sigma_y} \tag{3}$$

where σ_{xy} is the covariance of x (times-to-failure) and y (median ranks), σ_x is the standard deviation of x, and σ_y is the standard deviation of y.

Table 1: Correlation coefficient values

Feeder type	Correlation Coefficient Rho (ρ)
overhead +25%	0.985203
overhead	0.992959
underground +25%	0.975994
underground	0.964724
10 kV +25%	0.988244
10 kV	0.989144
35 kV +25%	0.972266
35 kV	0.983755
all feeders +25%	0.988580
all feeders	0.990089

The estimator of ρ is the sample correlation coefficient, given by:

$$\widehat{\rho} = \frac{\sum_{i=1}^{N} x_i y_i - \frac{\sum_{i=1}^{N} x_i \sum_{i=1}^{N} y_i}{N}}{\sqrt{\left(\sum_{i=1}^{N} x_i^2 - \frac{\left(\sum_{i=1}^{N} x_i\right)^2}{N}\right)\left(\sum_{i=1}^{N} y_i^2 - \frac{\left(\sum_{i=1}^{N} y_i\right)^2}{N}\right)}} \quad (4)$$

Weibull distribution function (5) is two-parametric distribution, with slope parameter η and shape parameter β.

$$F(t) = 1 - e^{\left(\frac{t}{\eta}\right)^{\beta}} \quad (5)$$

Slope parameter shows time at which 63.2% of analyzed units are failed. Shape parameter represents failure rate behavior. Its value tells whether failures are decreasing or increasing. $\beta<1$ indicates infant mortality, while $\beta>1$ shows wear out failures. Higher value of beta indicates greater rate of failure. Both β and η parameters are calculated for the whole CB population from the statistical data using the least square method [13]. Results are presented in Table II.

Weibull distribution function with right censored data (case when some devices didn't fail during period of analysis) unreliability is calculated for all CB's categories. On figures 2-5 unreliability distribution of different criterions is shown.

By observing Weibull parameters two conclusions could made, underground feeders (both criteria of voltage drop value limit) have highest β while overhead

Table 2: Weibull parameters

CB feeder type	η	β	Fail \Suspend
Overhead +25%	39.1	5.2	100 \87
Overhead	37.1	4.8	131 \56
Underground +25%	41.5	6.1	63 \169
Underground	38.1	6.1	97 \135
10 kV feeders +25%	43.4	5.6	87 \224
10 kV feeders	40.4	5.1	135 \176
35 kV feeders +25%	35.2	5.6	79 \31
35 kV feeders	33.8	5.6	96 \14

feeder have lowest value. Considering η parameter, 10 kV feeders (+25% limit voltage drop level) have closer time to failure, while 35kV feeders have lowest η value.
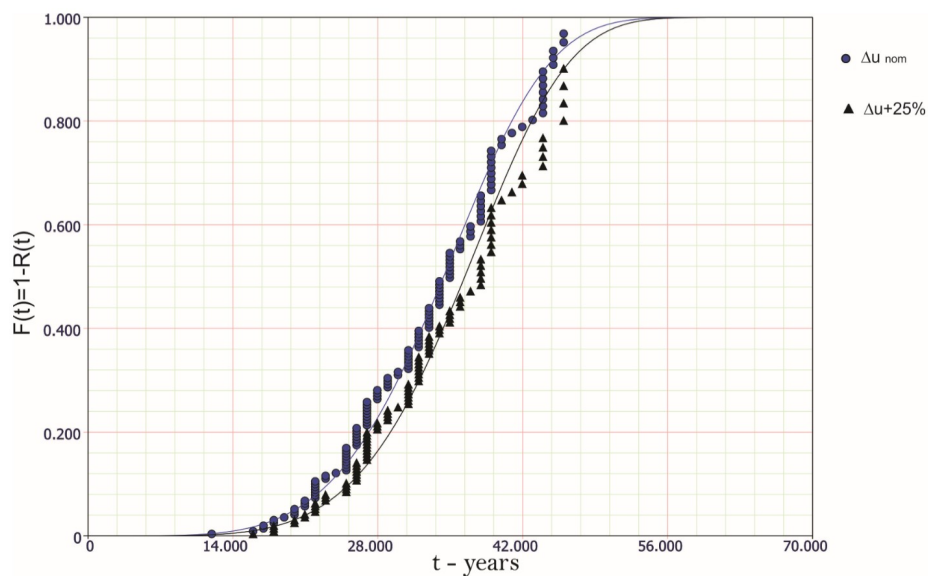
Figure 2: Weibull unreliability distribution for CB's on overhead feeders
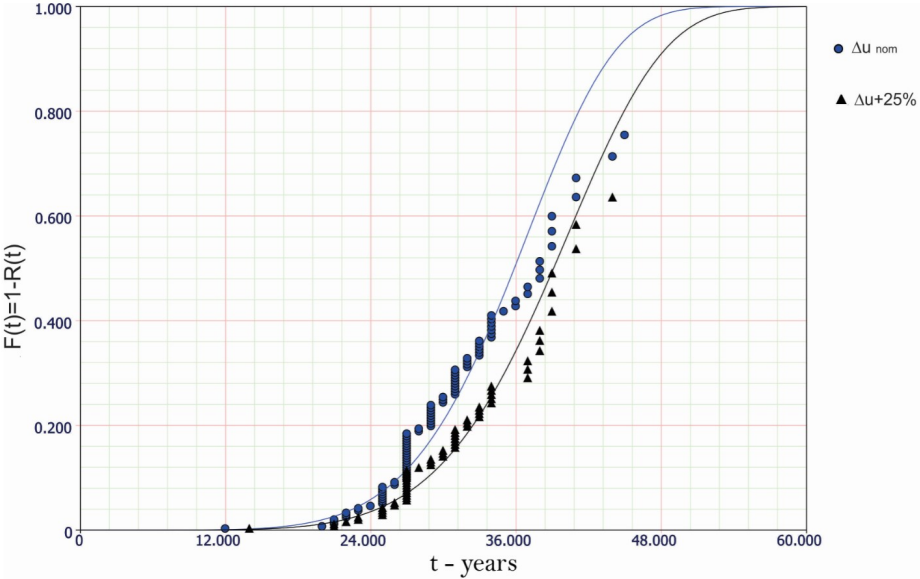
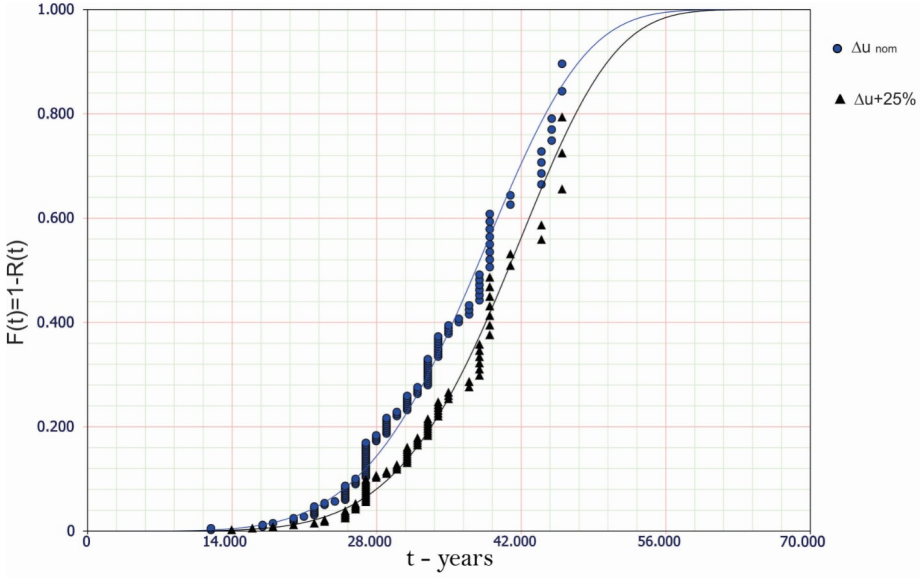Figure 3: Weibull unreliability distribution for CB's on underground feeders

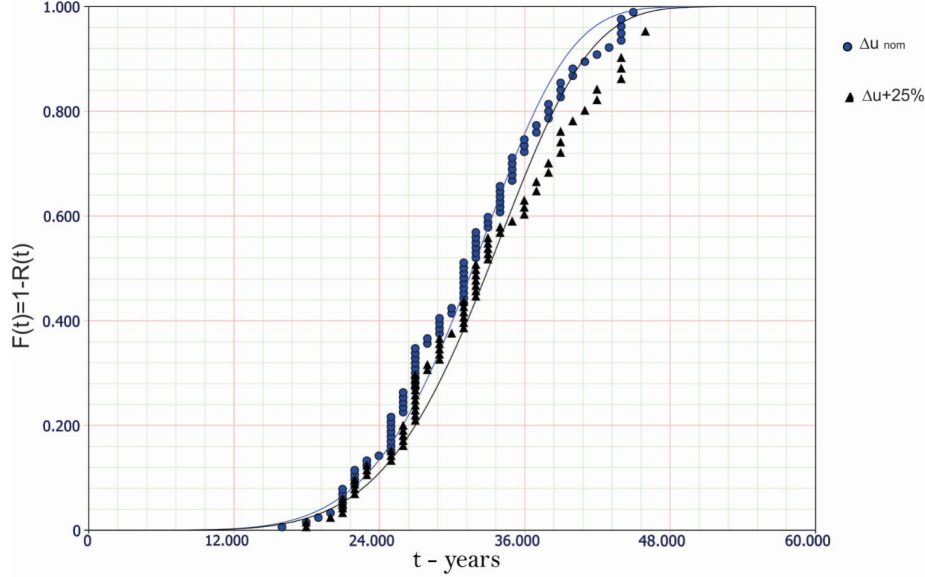Figure 4: Weibull unreliability distribution for CB's on 10 kV overhead feeders

Figure 5: Weibull unreliability distribution for CB's on 35 kV overhead feeders

3   Conclusion

The determination of CB remaining useful life is a complex procedure depending on various stochastic factors, including the current flowing through the CB, breaking current intensities, number of operations and operational conditions as well. In this methodology, RUL is determined implicitly, by the assessment of risk of failure from keeping the CB in operation, with the diversification of normal and abnormal operation conditions.

The total of 427 circuit breakers has been monitored, with data gathered in past 10 years. After the statistical tests, parameters for Weibull probability distribution of contact resistance for breakers on both overhead and underground feeders were determined. Weibull probability distribution of contact resistance for breakers on both overhead and underground feeders and voltage levels of 35 kV and 10 kV proved to be the best fit.

The proposed methodology requires historical data of different control parameter measurement and proved to be useful when the changes of breaker operational conditions are expected. The statistical analysis showed that the dominant feeder type (overhead or underground) has a great influence on probability of failure, and that these conditions must be taken into account in a quantitative way.

References

[1] Y. Hu, S. Liu, H. Lu, H. Zhang, "Remaining useful life assessment and its application in the decision for remanufacturing", Procedia CIRP, vol. 15, pp. 212–217, 2014.

[2] H. Picard, J. Verstraten, M. Hakkens, R. Vervaet, "Decision model for End of Life management of switchgears", El. and Instr. Appl. in the Petroleum & Chem. Ind., PCIC Europe 4th European Conference, Jun. 2007.

[3] C. Okoh, R. Roy, J. Mehnen, L. Redding, "Overview of Remaining Useful Life Prediction Techniques in Through-Life Engineering Services", Science Direct, Procedia CIRP, vol. 16, pp. 158 – 163, 2014.

[4] J. Z. Sikorska, M. Hodkiewicz, L. Ma, "Prognostic modelling options for remaining useful life estimation by industry", Mech. Syst. and sign. Process., vol. 25, no. 5, pp. 1803-1836, Jul. 2011.

[5] X. S. Si, W. Wang, C. H. Hu, D. H. Zhou, "Remaining useful life estimation – A review on the statistical data driven approaches", European Journal of Operational Research , vol. 2013, no. 1, pp. 1-14, Aug. 2011.

[6] J. F. Boudreau, S. Poirier, "End-of-life assessment of electric power equipment allowing for non-constant hazard rate – Application to circuit breakers", *El. Power and Energy Systems*, vol. 62, pp. 556-561, Nov. 2014.

[7] X. Zhang, E. Gockenbach, Z. Liu, H. Chen, L. Yang, "Reliability estimation of high voltage SF6 circuit breakers by statistical analysis on the basis of the field data", *El. Power System Research*, vol. 103, pp. 105-113, Oct. 2013.

[8] G. Balzer, F. Heil, P. Kirchesch, R. Meister, C. Neumann, "Evaluation of failure data of HV circuit-breakers for condition based maintenance", CIGRE, Paris, report A3-305, 2004.

[9] T. M. Lindquist, L. Bertling, R. Eriksson, "Circuit breaker failure data and reliability modelling", *IET Gen., Transm. & Distrib.* vol. 2, no. 6, pp. 813-820, Nov. 2008.

[10] Common specifications for high-voltage switchgear and control gear standards, International standard IEC 60694, Edition 2.2, 2002-01.

[11] Operating manual for medium voltage medium oil circuit breakers for internal assembly,Minel, Serbia, 1984.

[12] https://www.weibull.com/hotwire/issue71/relbasics71.htm; W. Li, J. Zhou, J. Lu, W. Yan "A Probabilistic Analysis Approach to Making Decision on Retirement of Aged Equipment in Transmission Systems" *IEEE trans. on power delivery*, vol. 22, pp. 1891–1896, no. 3, July 2007.

Dragan STEVANOVIĆ,
Electric Power Industry of Serbia,
Otona Župančiča 2, 11070 - Belgrade, SERBIA
E-mail: dragan985@gmail.com

Aleksandar JANJIĆ, Dragan TASIĆ,
University of Niš,
Faculty of Electronic Engineering,
Aleksandra Medvedeva 14, 18000 - Niš, SERBIA
E-mail: aleksandar.janjic@elfak.ni.ac.rs
E-mail: dragan.tasic@elfak.ni.ac.rs

EFFECTS OF EXTERNAL DIELECTRIC BODY ON PLAN-PARALLEL SYSTEM FIELD HOMOGENEITY

Zlata CVETKOVIĆ, Žaklina MANČIĆ, Saša ILIĆ,
Bojana PETKOVIĆ, Milka POTREBIĆ

Abstract

In this paper, it is presented the influence of an external cylindrical dielectric body on the homogeneous electrostatic field. To obtain a homogeneous electrostatic field, a system of four charged parallel electrodes was installed on the imaginary cylindrical surface of the radius R (primary cell of the first order). Expressions for the field within and outside the external body are obtained using the Image theorem in cylindrical dielectric mirror. Special attention was dedicated to the 2D view of the field in the cross-section of the system. [1]

Keywords and phrases: *dielectric cylindric, electrostatic systems, isotropic dielectric body, plan-parallel primary cell, uniform electrostatic field*

1 Introduction

The problem of generating homogeneous electric fields is quite old [1, 2] but still actual [3-10]. To generate a homogeneous field, charged rings [1, 3, 4, 6], systems based on plan-parallel electrodes [2, 5, 8-10], conical electrodes [4, 7], charged culotte [3], etc.

The influence of the external spherical body on the achieved homogeneity of the field in the example of rings was considered in [6], whereas the influence in the example of biconical systems is considered in [7]. An analysis of the influence of an external cylindrical conducting body on the achieved homogeneity of the field in the case of plan-parallel system is performed in [8], as well as in [10], where a special emphasis was placed on an external body made of bi-isotropic material.

In this paper, it is performed a detailed analysis of the influence of cylindrical external body made of isotopic dielectric material on the achieved homogeneity of

---

[1]PACS: S2.35.Fp; 78.20.Ci

the field, which is generated using a system of two pairs of electrodes which are loaded with the same amount of charges per unit length but of opposite sign.

System dimensions are selected so that a homogeneous electrostatic field is obtained in the central region of the system (plan-parallel first-order cell). The emphasis of the paper is on the qualitative representation of the field distribution in the cross-section of the observed system.

2   Image theory for the dielectric cylinder

In Figure 1, it is shown the cross-section of the system, consisting of the primary plan-parallel cell of the first order, which is used for generating homogeneous electrostatic field [5] and external dielectric body of cylindrical shape in homogeneous field, whose axis coincides with z-axis od the system. Dimensions of the primary cell are $h/R = \cos(\alpha)$ and $d/R = \sin(\alpha)$[5], where R represents the radius of the imaginary cylinder according to which are placed the plan-parallel charged electrodes. Parameter a is the radius of the dielectric body permittivity $\varepsilon = \varepsilon_0 \varepsilon_r$, while the exterior medium is assumed to be air,

$$\varepsilon_0 = \frac{10^{-9}}{36\pi} \; \frac{\text{F}}{\text{m}}.$$
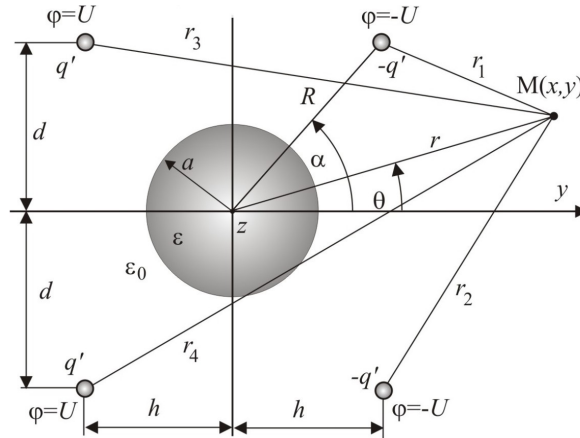

Figure 1: Cross section of the plan parallel primary cell with external dielectric body

In the case when the external body does not exist the potential φ, at the point M, is given by

$$\varphi(x,y) = \frac{q'}{2\pi\varepsilon} ln\frac{r_1 r_2}{r_3 r_4}, \tag{1}$$

where r_1, r_2, r_3 and r_4 denote the distances between the axis of primary cell conductors and observed point.

In the case when $\alpha = \pi/3$ in the central region of the primary plan-parallel cell of the first order, electric field is practically homogeneous and equal to [5]:

$$E(0,0) = \frac{q'\sqrt{3}}{\pi\varepsilon R} \tag{2}$$

When the Image theorem is applied in dielectric cylindrical mirror for the system in Figure 1, then the equivalent charge system that generates an electric field in the area outside the cylinder ($r>a$), consists of original charges per unit length q' and -q' and their images $\beta q'$ and $-\beta q'$, positioned along the cylindrical surface of the radius $D = a^2/R$ in the air, ε_0 (Figure 2). Constants A and B depend on the permitivity of the cylindrical body [12]

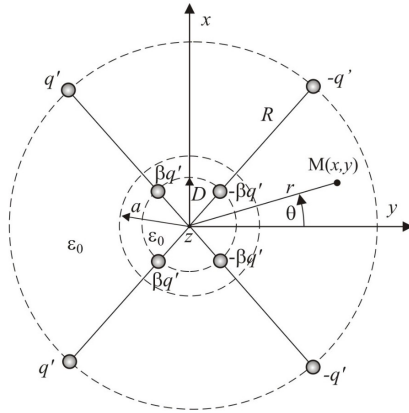$$\beta = \frac{\varepsilon_0 - \varepsilon}{\varepsilon_0 + \varepsilon} \tag{3}$$

Figure 2: Equivalent system of charges and their images in the air for determining the electric field in the area outside the cylinder $r > a$

For the calculation of the electric field inside the dielectric cylinder ($r<a$), the equivalent charge system is placed in the dielectric medium, and it consists of

images $\gamma q'$ and $-\gamma q'$, located at the positions of the original conductors of the plan-parallel cell, Figure 3, where

$$\gamma = \frac{2\varepsilon}{\varepsilon_0 + \varepsilon}. \tag{4}$$
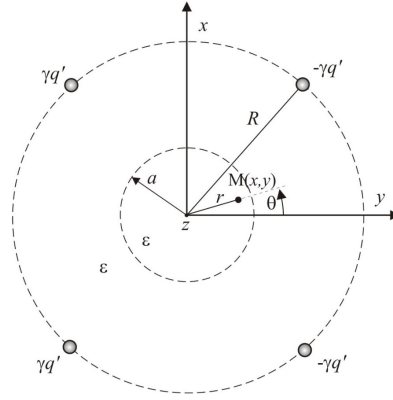

Figure 3: Equivalent charge system placed into dielectric for determining electric field in the region inside cylinder, $r < a$

The procedure for determining the field inside dielectric cylinder, placed in a homogeneous field is described by using the cylindrical coordinate system (r, θ). The function of scalar potential inside the cylinder in homogenous electric field of intensity $E(0,0)$, is described as it follows:

$$\varphi = -\frac{2\varepsilon}{\varepsilon + \varepsilon_0} r\, E(0,0) \cos\left(\theta\right),\ \ for\ \ \ r \leq a. \tag{5}$$

As $y = r \cos\left(\theta\right)$ in the coordinate system in Figure 1, the field inside the cylinder is homogenous and it has y-component only.

$$E_y = \frac{2\,\varepsilon}{\varepsilon + \varepsilon_0} E(0,0). \tag{6}$$

Thus, the field inside the dielectric cylinder is homogeneous and less than the field outside the cylinder.

Figure 4 and 5 - *2D presentation of the normalized electric field for plan parallel primary cell without and with external body*
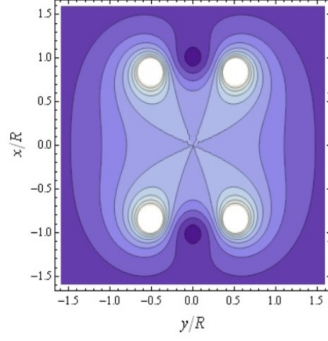
Figure 4: Normalized electric field for plan parallel primary cell without body
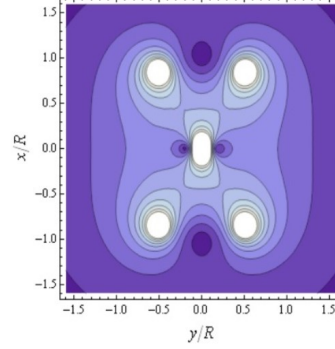
Figure 5: Normalized electric field for plan parallel primary cell with perfectly conducting body
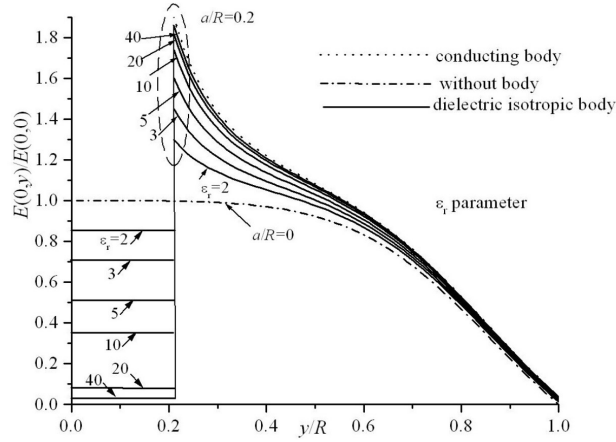

Figure 6: Normalized electrostatic field along y - axis of the system with external dielectric cylindrical body, for different values of ε_r

3   Numerical results

In the present paper, for generating homogeneous electrostatic field is exploited primary cell of the first order whose dimensions are $h/R = 0.5$ and $d/R \cong 0.866$[5]. In Figure 4 it is shown 2D distribution of the generated homogeneous electric field, $E(x,y)/E(0,0)$, for the system in Figure 1 in the case without external body,

whereas the case when external conducting body of cylindrical shape and radius $a/R = 0.2$ is placed in the center of the system is shown in Figure 5 [8, 10]. The conducting body in its vicinity disrupts homogeneity of the field, whereas inside the conducting body the field is equal to zero.

Figure 6 shows normalized values of the electric field intensity along the axis of the system in the case when dielectric body is inserted in homogeneous field and placed as in Figure 1, where dielectric constant of the body, ε_r, is a parameter [10]. It can be noticed that as the dielectric constant increases, the intensity of the field inside the body decreases and tends to zero, whereas outside the dielectric cylinder the intensity of the field converges as in the case of the conductive body.

In order to better understand the extent to which the dielectric constant of the body affects the achieved homogeneity of the field, in the same figure it is shown the normalized ratio of the electric fields in the absence of a external body, as well as in the presence of a perfectly conductive external body. The obtained results show that, in electrostatic terms, dielectrics with a large dielectric constant can be considered as conductors (ε_r>40), and vice versa, that perfect conductors can be considered as a dielectric whose dielectric constant in ideal case tends to infinity.

2D distribution of the electric field in the cross-section of a system for generating a homogeneous electric field with an external body of the radius $a/R = 0.2$, in the case when $\varepsilon_\mathrm{r} = 2$ is shown in Figure 7, whereas the case $\varepsilon_\mathrm{r} = 50$ is shown in Figure 8.

By comparing the obtained results, it can be seen that in the case $\varepsilon_\mathrm{r} = 50$, field distribution is approximately the same as in the case of the conductive body, Figure 5, which can be explained by the fact that due to large dielectric constant, a dielectric body behaves approximately like a conductive body.
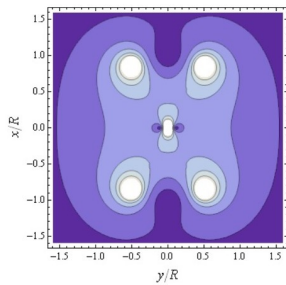

Figure 7: Normalized electric field in the presence of external body ($\varepsilon_\mathrm{r} = 2$)
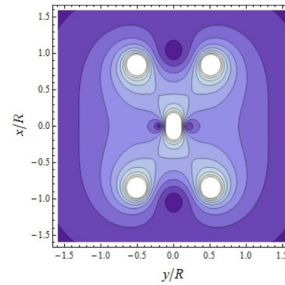
Figure 8: Normalized electric field in the presence of external body ($\varepsilon_\mathrm{r} = 50$)

Figure 7 and 8 - *2D presentation of the uniform electric field for plan-parallel primary cell with dielectric body of radius $a/R = 0.2$ when: a) $\varepsilon_r = 2$;b) $\varepsilon_r = 50$.*

In Figure 9 it is shown distribution of the electric field inside and outside the external body of dielectric constant $\varepsilon_r = 2$ for various dimensions of external body, a/R. As it could be expected, the body of larger dimensions disrupts the homogeneity of the field in its vicinity to the larger extent, whereas inside the body the field is homogeneous and it is lower than the field intensity on the surface of the body.
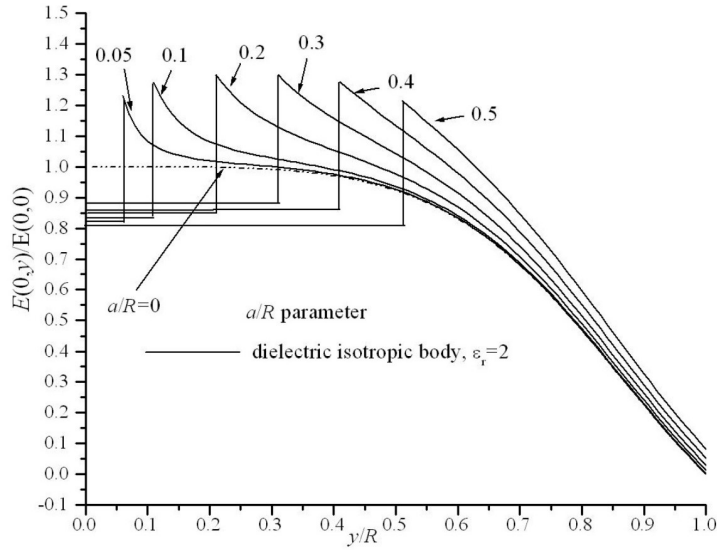

Figure 9: Normalized electric field along y axis using one primary cell without and with dielectric cylindrical body for different dimensions a/R and $\varepsilon_r = 2$

4   Conclusion

In this paper, we have analyzed the influence of the external dielectric cylindrical body, placed in the center of the plan-parallel cell of the first order, on the achieved homogeneity of the field. By using Image theorem in cylindrical dielectric mirror we have obtained equivalent system of charges to determine the field inside and outside of the external body.

It is considered 2D distribution of electric field in the following cases: without external body in the homogeneous field and when there is an external body. In

the second case, the body can be made using dielectric materials of various permeabilities or it can be conducting body. We have observed how various types of dielectrics and dimensions of the body disrupts achieved homogeneity.

As it could be expected, electric field inside conducing body, which is placed in homogeneous electric field, is equal to zero, whereas the field iz homogeneous and less than the field outside the body inside dielectric body.

Also, it can be noted that with increasing dielectric constant of the external body, achieved homogeneity is disrupted to the larger extent, and that distribution of the field tends to the distribution of the field in the case of conducting body of the same dimensions.

4.1   Acknowledgement

References

[1] M.W. Garrett, "Axially Symmetric Systems for Generating and Measuring Magnetic Fields", Prt I. J. Appl Phys, vol. 22. Pp. 1091-1107, 1951.

[2] C.E. Baum, "Impedances and Field Distributions for Symmetrical Two Wire and Four Wire Transmission Line Simulators", Sensor and Simulation, Note 27, Oktober 1966.

[3] J.A. Jungerman, "Fourth-order Uniform Electric Field from Two Charged Rings", Rev. Sci. Instrum., vol 55, pp. 1479-1482, 1984.

[4] D.M. Velieković, Z.Ž. Cvetković, "Systems for Generating of Homogeneous Electrical Field", Facta Universitatis, series Electronics and Energetics, Vol.14, no. 1, pp. 93-106, 2001.

[5] Z.Ž. Cvetković, "*Homogeneous electric and magnetic field generation*", PhD thesis, Faculty of Electronic Engineering, Niš, 2001. (in Serbian).

[6] Z.Ž. Cvetković, B. R. Petković, M. T. Perić, "Systems for Homogeneous Electrical Fields Generation and Effects of External Bodies on Field Homogeneity", Applied Computational Electromagnetics Society Journal, vol. 26, No. 1, pp. 56-63, January 2011.

[7] Z.Ž. Cvetković, S.R Aleksić, M.T. Perić, B.R. Petkovi'c, "Influence of the Conducting Body on the Biconical Electrode Field", The second European Conference on Antennas and Propagation-EuCAP 2007, CD-Proceedings (ThPA.025), Edinburg, United Kingdom, November 11-16, 2007.

[8] Z.Ž. Cvetković, M.M. Potrebić, "Influence of Conducting Body on the Plan-Parallel Electrode Field",Proceedings of 12th International Conference on Telecommunications in Modern Satellite, Cable and Broadcasting Services, (TELSIKS), Serbia, Nis, ECIT.8, pp. 350-353, 14-17 October 2015.

[9] Z.Ž. Cvetković, M.M. Potrebić, "Stability analysis of plan-parallel systems for uniform electrostatic field generation", XII International SAUM Conference on Systems, Automatic Control and Measurements, pp. 308–311, Niš, Serbia, November 12–14, 2014.

[10] Z.Ž. Cvetković, Ž. Maneić, M. Potrebić, S. Ilić, Effects of external bodies made of different materials on plan-parallel system field homogeneity, Revue Romaine des sciences techniques, Series electrotechnique and energetique, Romanian Academy, Publishing House of the Romanian Academy, Vol. 64, no. 1, pp. 3-8, 2019.

[11] I.V. Lindel, "Static image method for layered isotropic and Biisotropic cylinders", Microwave and Optical Technology Letters,*6*, pp. 383-387, 1993.

[12] D. M. Velieković, "Calculation methods for electrostatic fields", Stil, 1999.(in Serbian).

Zlata CVETKOVIĆ, Žaklina MANČIĆ, Saša ILIĆ,
University of Niš,
Faculty of Electronic Engineering,
Aleksandra Medvedeva 14, 18000 - Niš, SERBIA
E-mail: zlata.cvetkovic@elfak.ni.ac.rs
E-mail: zaklina.mancic@elfak.ni.ac.rs
E-mail: sasa.ilic@elfak.ni.ac.rs

Bojana PETKOVIĆ,
Ilmenau University of Technology,
Faculty of Electrical Engineering and Information Technology,
P.O. Box 100565, D-98684 Ilmenau, GERMANY
E-mail: bojana.petkovic@tu-ilmenau.de

Milka POTREBIĆ,
University of Belgrade,
School of Electrical Engineering,
Bulevar kralja Aleksandra 73, 11120 - Belgrade, SERBIA
E-mail: milka_potrebic@etf.rs

VISUALISATION OF STATIC AND STATIONARY MAGNETIC FIELDS

Branko KOPRIVICA, Alenka MILOVANOVIĆ, Srdan DIVAC,
Mihajlo TATOVIĆ, Milan PLAZINIĆ, Vojislav VUJIČIĆ

Abstract

The aim of this paper is to present a way of visualisation of the magnetic field created by permanent magnets or wires and loops carrying direct current. Visualisation is achieved by using so called magnetic field viewer - a special magnetic sensing film. Except visualisation of the magnetic field around the magnetic object, measurements of magnetic flux densities are performed using a Hall sensor. Also, a number of simulations of coils carrying direct current in FEM software have been made in order to check a validation of the visualisation effects obtained. The paper shows photographs of visualised magnetic fields and the results of measurements and simulations, as well as a proper discussion. [1]

Keywords and phrases: *hall sensor, magnetic field viewer, static and stationary magnetic field, visualisation*

1 Introduction

Magnetic fields can be created by permanent magnets or conductors carrying direct current, while its presence can be observed by appearance of force on other magnets or conducting bodies placed inside the field [1]. However, the magnetic field distribution cannot be easily seen, while it can be calculated or simulated [1]. One way of magnetic field visualisation is to use ferro fluids [2]. Also, with the aim of field visualisation, magnetic field viewing films were produced [3]. They show the magnetic field by showing its location and direction. Magnetically sensitive nickel particles in this film change their positions based on the intensity and orientation of the applied magnetic field. The particles will be shown as brighter regions if the magnetic field is parallel to the surface of the film and darker regions

---

[1]PACS: 07.55.Db

if the field is orthogonal to the film surface [2]. The shade of these regions depends on the intensity and direction of the magnetic field.

Experiments were conducted with permanent magnets and coils of different shapes. A photograph of permanent magnets and photographs of a magnetic viewer placed above these magnets and coils are presented in the paper, as well as a proper discussion. A part of the results obtained for coils carrying direct current is compared with the results obtained by FEM software. Moreover, results of measurements of magnetic flux density using a Hall sensor are given in the paper.

2   Theoretical Approach

Neodymium permanent magnets have been used for creating a static magnetic field [4], while coils carrying direct current have been used for creating stationary magnetic field. Different values of direct currents have been set in order to obtain different intensities of magnetic field created. These fields have been visualised with the magnetic field viewer, by placing it above the magnets and coils. Hall sensor has been used for measurement of magnetic flux density around the coils. FEM software has been used for simulations of magnetic field produced by coils. Geometry of coils, number of turns and values of direct current in the simulations were identical as for the real experiments performed with coils.

2.1   Results

Figure 1 shows a photograph of arrangement of permanent magnets used in the experiment, as follows: two magnets of the square surface placed next to each other, one curved magnet and fifteen cylindrical magnets placed next to each other. Figure 2 shows a photograph of a magnetic viewer placed above permanent magnets from Figure 1. It can be seen from Figure 2 that surfaces of the magnets, as well as the close surroundings of the magnets, are shaded dark, while the areas between magnets or close to its edges are much brighter (for two magnets with square surface). In the case of curved magnet bright line can be seen in the middle, which means that this magnet actually consists of two magnets (this cannot be observed by usual visual inspection).

On the other hand, for the arrangement of cylindrical magnets bright lines do not appear in the places where magnets touch each other, but they appear in the places slightly closer to the touching surfaces between magnets and magnetic film. Thus, appearance of darker or brighter regions and lines depends also on the shape of the magnet.

Figure 3 shows the photographs of the magnetic viewer placed above arrangement of two square permanent magnets (12 mm by 12 mm, 5 mm high) used in
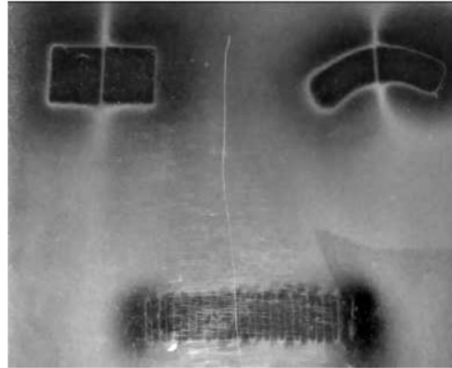
Figure 1: *Photograph of permanent magnets*

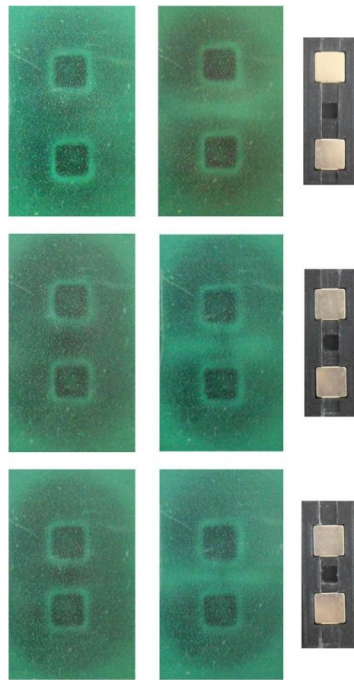Figure 2: *Photograph of magnetic viewer placed above permanents magnets*

Figure 3: *Photographs of permanent magnets inside plastic holder and corresponding photographs of magnetic viewer when magnets attract and repel*

the experiment, as follows: two magnets of square surface placed in plastic holders with three different sizes of gap (15 mm, 20 mm and 25 mm) between these magnets (in the right side). Magnets have been arranged so that in one case they attract each other and in another case they repel. Both cases have been visualised with magnetic viewer and the corresponding photographs are presented in Figure 3. Left part of the figure shows magnetic field of the magnets when they repel and middle part shows magnetic field of the magnets when they attract.

One significant difference can be observed in the area between two magnets. During the repelling, magnetic viewer shows a dark area between magnets, which means that the magnetic field is almost normal to the plane of magnetic viewer. The same area is mostly bright during the attraction, which means that the magnetic field is almost parallel to the plane of magnetic viewer.

Two coils have been made by winding a copper wire on plastic holders of circular and square cross-section. A diameter of the circular holder was 30 mm and 18 windings has been wound, while one side of the square holder was 25 mm and 17 windings has been wound. Height of both coils is 5 mm.

Figure 4 shows the photographs of magnetic viewer placed above coils with circular and square shape obtained for different values of direct currents from 0 to 20 A, in steps of 5 A (0 on the top and 20 A at the bottom). These photographs show a gradual increase of intensity of the dark area, corresponds to the internal area constrained by the coil, which indicates the appearance of magnetic field mostly normal to the plane of magnetic viewer. This dark area is surrounded by brighter area, corresponds to the area of the coil itself, which indicates a presence of a mostly horizontal magnetic field. Outside of this brighter area there is again darker area, but with lower intensity.

Models of coils of the same geometry and number of turns as real coils have been created in FEM software, as it is presented in Figure 4 for square coil.

A number of simulations have been made with the same values of direct current as for actual experiments. Several results have been obtained from these simulations, such as: plots of magnetic flux density in the horizontal plane just above the coil, the plot of the magnetic flux density vector in the vertical plane and graph of horizontal and vertical component of magnetic flux density in the vicinity of the coil. Plots of magnetic flux density in the horizontal plane (xyplane in Figure 5) have been grouped in the same manner as for the experiment and they are presented in Figure 6. These plots are very similar to photographs given in Figure 4 and they confirm previously made observations of magnetic field around the coil.

Figure 7 presents plot of magnetic flux density vector in the vertical plane (xz plane in Figure 5) that contains the vertical axis of square coil. This plot shows that inside internal area surrounded by the coil the vector of magnetic flux density
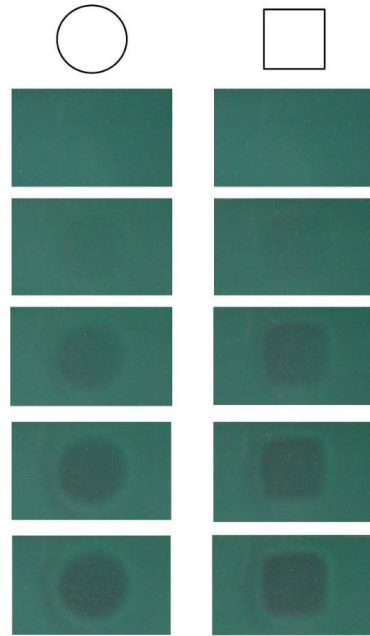
Figure 4: *Photographs of magnetic viewer above circular and square coil with direct current of different levels*
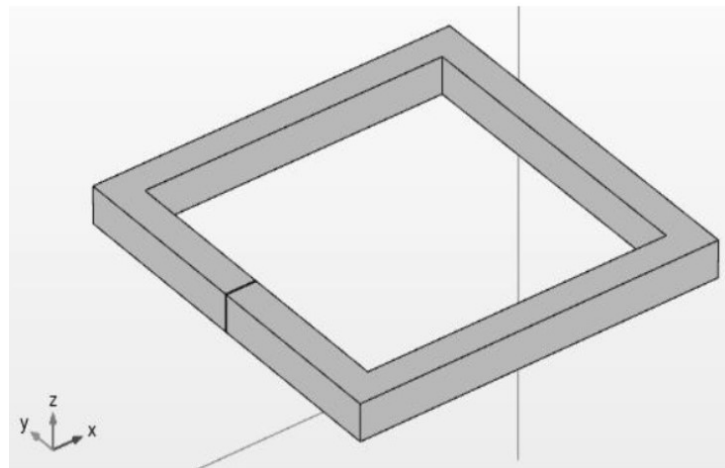

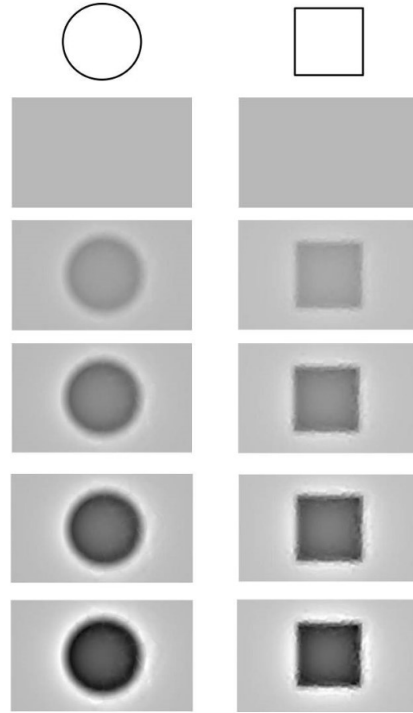Figure 5: *Model of square coil*

Figure 6: *Plots of magnetic flux density obtained from simulations*

is vertical, while closer to the coil it changes direction and just above the coils it becomes horizontal. Furthermore, it can be observed that vector is also vertical outside the coil, but with smaller intensity. All this supports observations given for photographs in Figure 4.

Figure 8 presents variation of horizontal B_x and vertical B_z component of magnetic flux density across the horizontal line parallel with y axis, at height z equal to half of height of coil (Figure 9). Graphs in Figure 8 have been obtained at direct current of 10 A.

Several measurements of magnetic flux density have been made with both coils in order to check the quality of simulation. Hall sensor has been placed in the centre of the coils, at the height equal to the half of the height of the coil. Direct current has been set to 5 A and 10 A in these measurements. The results of the vertical component of magnetic flux density are given in Table I. The relative difference between results obtained is around 3 % for circular coil and around 12 % for square coil.

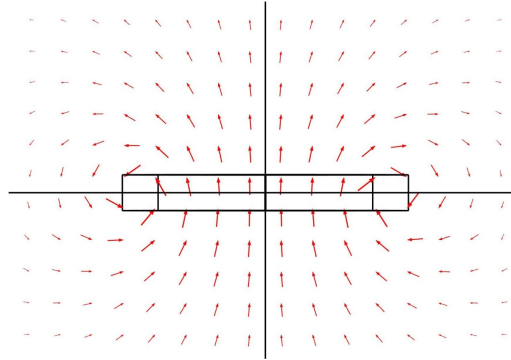This difference is acceptable and measurements confirm simulations, even for

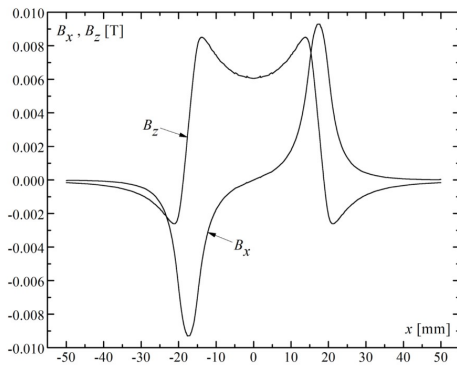Figure 7: *Vector plot of magnetic flux density around square coil*

Figure 8: *Variation of magnetic flux density components: circular coil*
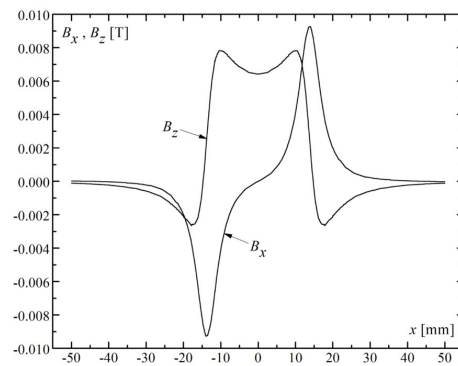
Figure 9: *Variation of magnetic flux density components: square coil*

square coil where difference is higher. Such result can be expected since real coil is not a real square and it is not produced with high precision.

3   Discussion

Several advantages and disadvantages in application of magnetic viewer have been observed during performed experiments. The advantages are: fast "reaction" on the gradual variation of magnetic field created by the coils and stability of the shade and good reproducibility. The disadvantages are: relatively high level of lowest magnetic field that can be detected (starting from about 1000 A/m), effect of saturation - at higher magnetic field viewer almost stops to be darker and
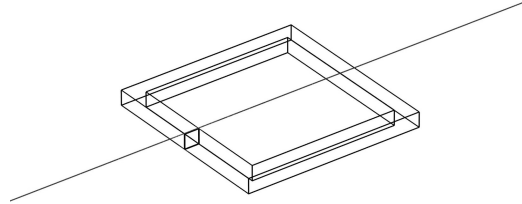
Figure 10: *Horizontal line above square coil*

Table 1: Comparison of measured and simulated results for vertical component of magnetic flux density

I [A]	B_z [mT]			
	Square		Circle	
	Hall	FEM	Hall	FEM
5	2.89	3.35	3.05	3.14
10	5.92	6.70	6.13	6.29

darker, glossy surface reflects light from point sources (like flashes and lamps) - so it is not easy to make a proper photograph, plastic foil is not resistant to high temperatures, bending and scratching, parts of the viewer disposed to magnetic field stays slightly dark after removing of magnet or coil - erasing of dark spots is needed.

An improvement of the experiment described could be made if digital camera and personal computer with adequate software for image acquisition and processing were used. The idea would be to capture a photograph of magnetic viewer placed above the magnetic object that creates known or measurable magnetic field. In the next step, the software would calculate the shade and link it with a certain value of magnetic flux density. Up to ten such measurements would be enough to perform calibration of magnetic viewer. Later, non-uniform magnetic field of other objects could be measured/calculated by processing of photograph.

4   Conclusion

This paper presents the results of visualisation of magnetic field created by permanent magnets and coils carrying direct current. This has been achieved using magnetic field viewing film - flexible sheet coated with nickel particles. Coils of the same geometry and number of turns have been simulated in FEM software and results of simulations have been presented. Furthermore, results of measurements of magnetic flux density around coils have also been presented. A proper discussion of all results has been given.

Magnetic viewing film can be successfully used for educational purposes, while its application in real scientific research need to be further examined.

References

[1] K. L. Kaiser: "Electromagnetic compatibility handbook", CRC Press, NY, USA, 2004.

[2] Y. Qingxin, F. Yanqing, S. Qiao, L. Xuehui: "A new method of showing magnetic field based on ferrofluid", Physics Procedia, Vol. 9, 2010, pp. 210-215.

[3] https://magnametals.co.uk/products/magnetic-field-view-film.

[4] https://www.stanfordmagnets.com/the-strongest-permanent-magnet-neodymium-magnet.html.

Branko KOPRIVICA, Alenka MILOVANOVIĆ, Srdan DIVAC,
Mihajlo TATOVIĆ, Milan PLAZINIĆ, Vojislav VUJIČIĆ,
University of Kragujevac,
Faculty of Technical Sciences Čačak,
Svetog Save 65, 32000 - Čačak, SERBIA
E-mail: branko.koprivica@ftn.kg.ac
E-mail: alenka.milovanovic@ftn.ac.rs
E-mail: divacsrdjan@gmail.com
E-mail: mihajlo.tatovic@ftn.kg.ac.rs
E-mail: milan.plazinic@ftn.kg.ac.rs
E-mail: vojislav.vujicic@ftn.kg.ac.rs

INSTRUCTIONS FOR THE AUTHORS

The "Buletinul Ştiinţific al Universităţii Politehnica Timişoara" is a direct successor of the "Buletin scientifique de l'École Polytechnique de Timişoara" which was started in 1925. Between 1982 – 1989 it was published as the "Lucrările Seminarului de Matematică şi Fizică ale Institutului Politehnic "Traian Vuia" din Timişoara".

Publication program: one volume per year in two issues, each series.

The "Mathematics-Physics" series of the "Buletinul Ştiinţific al Universităţii Politehnica Timişoara" publishes original papers in all areas of the pure and applied mathematics and physics.

1. The manuscript should be sent to the Editor, written in English (or French, or German, or Russian). The manuscript should be prepared in LATEX.
2. Maximum length of the paper is 8 pages, preferably in an even number of pages, in Times New Roman (12 pt).
3. For the first page the authors must bear in view:
    - an Abstract single spaced (at most 150 words) will be placed before the beginning of the text as: ABSTRACT. The problem of …
    - footnote with MSC (Mathematics Subjects Classification) or PACS (Physics Abstracts Classification System) Subject Classification Codes (10 pt)
4. Graphs. illustrations and tables should placed into the manuscript (send it as .eps or .pdf file), with the corresponding consecutively number and explanations under them.
5. The complete author's (authors') address(es) will be placed after References.
6. A Copyright Transfer Agreement is required together with the paper. By submitting a paper to this journal, authors certify that the manuscript has not been submitted to, nor is it under consideration for publication by another journal, conference proceedings, or similar publications.
7. There is no page charge and after registration a paper is sent to two independent referees. After acceptance and publication the author will receive 5 reprints free of charge. If a larger amount is required (fee of 2 USD per copy per article) this should be communicated to the Editor.
8. Manuscripts should be sent to:

For Mathematics

Dr. Liviu CĂDARIU
POLITEHNICA UNIVERSITY TIMISOARA
Department of Mathematics
Victoriei Square, No. 2
300006 – TIMIŞOARA, ROMANIA
liviu.cadariu-brailoiu@mat.upt.ro

For Physics

Dr. Dušan POPOV
POLITEHNICA UNIVERSITY TIMISOARA
Department of Physical Fundamentals
of Engineering
B-dul. V. Parvan, No.2
300223 – TIMIŞOARA, ROMANIA
dusan.popov@et.upt.ro